Hindawi
Shock and Vibration
Volume 2023, Article ID 8851565, 23 pages
https://doi.org/10.1155/2023/8851565

Research Article

Optimal Intensity Measures for Probabilistic Seismic Stability Assessment of Large Open-Pit Mine Slopes under Different Mining Depths

Wei Che, Pengfei Chang, and Wenhao Wang

School of Engineering and Technology, China University of Geosciences, Beijing 100083, China

Correspondence should be addressed to Wei Che; chewei@cugb.edu.cn

Received 22 January 2023; Revised 15 March 2023; Accepted 22 March 2023; Published 4 April 2023

Academic Editor: Letícia Fleck Fadel Miguel

The dynamic stability of slopes is the key to ensure the safety of a large open-pit mine during and after a strong earthquake. This study was mainly focused on the identification of optimal intensity measures (IMs) for the probabilistic seismic stability assessment of large open-pit mine slopes within the framework of performance-based earthquake engineering (PBEE). To this end, four open-pit slopes with different mining depths were constructed as the reference cases for the numerical investigation. The randomness of input ground motions and the uncertainty of material properties of the slopes were also considered. A total of 96 ground-motion records and 29 common IMs were selected for testing. By a series of nonlinear time-history analyses, the probabilistic seismic demand models (PSDMs) between the minimum factor of safety (FOS) of slopes and all considered IMs were developed. The optimal IMs with respect to FOS were identified based on the evaluation of five criteria: correlation, efficiency, practicality, proficiency, and sufficiency. The impacts on seismic fragility and FOS response hazard of the slopes were discussed when using different IMs. The results reveal that sustained maximum velocity (SMV) and velocity spectrum intensity (VSI) are recognized as the optimal IM for a mining depth of 50 m and 100 m, respectively. However, Housner intensity (HI) is observed to have the best predictability for both the mining depths of 200 m and 300 m. Moreover, for the three most commonly used IMs, peak ground velocity (PGV) is superior to peak ground acceleration (PGA) and spectral acceleration at first mode period (Sa (T_1)) for different mining depths. Finally, based on the evaluations of seismic fragility and FOS response hazard, the uncertainty of seismic stability prediction of open-pit slopes can be greatly reduced when using a more appropriate or optimal IM.

1. Introduction

Slope engineering is an important safety project in large open-pit mine. The slope stability is a key technical issue for the production safety of mine and has always been one of the research focuses in geotechnical and earthquake engineering. With the increase of mining depth and slope height, the stability and safety of slope is reduced in the mining process of deep concave open-pit mine. It would unleash a host of geological disasters such as landslide and collapse. There are many factors affecting the slope stability such as geology and geomorphology, hydrological condition, climate condition, stratigraphic lithology, and tectonic activity [1]. Strong earthquakes caused by tectonic activities could greatly increase the slope instability and have been recognized as a major cause of landslides. Because the slope disasters triggered by strong earthquakes have the characteristics of strong abruptness, wide spread, great destruction, and difficult defense, it is easy to cause serious damage of engineering structures near the slope or even directly be buried, which seriously threatens the lives and property of miners. Many cases for severe damage of slopes and even collapse have been reported in many literatures. The 1994 Northridge earthquake ($M_w = 6.7$) induced more than 11,000 landslides over an area of about 10,000 km^2 and led to as much as 30 billion in losses [2]. During the 1995 Great Hanshin earthquake ($M_w = 6.9$), about 60 landslides occurred around Awaji Island and the northern mountains of Kobe City [3]. The area of the slope disasters caused by the 1999 Chichi earthquake ($M_w = 7.6$) accounted for 3% of the area of

Taiwan [4]. The 2008 Wenchuan earthquake ($M_w = 7.9$) caused more than 15,000 landslides, collapses, and other slope disasters [5]. Therefore, it is of paramount importance to accurately predict the seismic responses and evaluate the seismic risk of large open-pit mine slopes when subjected to a strong earthquake. These evaluations would help to improve the seismic design of open-pit slopes and ensure their stability and safety in future earthquakes.

There are many uncertainties involved in evaluating the dynamic stability and seismic risk of open-pit slopes, including spatial variability of soil-rock properties and unpredictable characteristics of bedrock ground motions [6]. Most of the traditional methods for seismic dynamic stability of slopes are usually adopted deterministic analyses based on a few earthquake records [7, 8]. The deterministic analyses cannot fully consider the effect of these uncertainties, resulting in the inability to accurately predict the seismic failure behavior of slopes. The performance-based earthquake engineering (PBEE) developed by the Pacific Earthquake Engineering Research (PEER) Center is an advanced probabilistic seismic risk assessment methodology and can provide more rational, credible, and practical way to quantify the inherent uncertainties of all performance variables of slopes. The PBEE framework has been currently applied to the seismic risk assessment of various civil engineering structures such as buildings [9], bridges [10], dams [11], and towers [12]. However, limited numbers of literature are available on probabilistic seismic stability assessment of slopes based on the advanced PBEE methodology [13], especially to open-pit mine slopes.

Probabilistic seismic demand model (PSDM) is one of the crucial components of the seismic risk assessment of slopes when using the PBEE framework [14]. PSDM describes the probabilistic relationship between engineering demand parameter (EDP) of slopes and input ground-motion intensity measure (IM). It can be formulated by performing the probabilistic seismic demand analysis (PSDA) of slopes. Subsequently, seismic fragility curves can be developed based on the constructed PSDM of slopes [15]. Seismic fragility curves reflect the conditional probability of a slope reaching or exceeding the predefined damage limit states for a given IM level. In addition, fragility curves can provide richer and comprehensive expression for seismic damages of slopes than only failure probability obtained by traditional reliability methods because they are described in the form of certain functions rather than points [16–18]. The selection of an appropriate or optimal IM is one of the key prerequisites to reduce the uncertainty of the PSDM and obtain reliable fragility curves of slopes [19]. An appropriate IM would be able to represent certain key characteristics of amplitude, frequency content, duration, and energy of ground motions, accurately predict the seismic responses, and reduce the variance of dynamic damage assessment of slopes [20]. In engineering practice, peak ground acceleration (PGA), peak ground velocity (PGV), and spectral acceleration at first mode period (Sa (T_1)) are often selected as the most commonly used IMs based on experiences to construct the PSDM and fragility curves of slopes. However, several studies have reported PGA, PGV, and Sa (T_1) are not always the best IMs to predict the seismic responses of slopes [21]. Meanwhile, the best IM for seismic demand analyses may vary greatly depending on the slope type, local soil and rock conditions, or even the EDPs used in the analysis. Therefore, there is no clear consensus on which IM is recommend as the optimal IM for slopes.

Several evaluation criteria have been proposed to determine the best IM for seismic risk assessment of various structures, including correlation, efficiency, practicality, proficiency, sufficiency, relative sufficiency, and hazard computability. To date, these criteria and extensive studies are mainly focused on buildings [22, 23], bridges [24], dams [25], storage tanks [26], tunnels [27, 28], offshore platform [29, 30], and nuclear power plant [31, 32]. Due to the space constraints, an elaboration of the work about optimal IM for above-given structures is not shown herein. Significantly, there are a few previous studies investigated the correlation between a small amount of IMs and seismic permanent displacement of slopes using Newmark sliding block model (NSBM) [33, 34]. They found the best IM for seismic displacements of slopes is spectral acceleration at 1.5 times first mode period (Sa ($1.5T_1$)) because the nonlinearity of soil and rock mass leads to the elongation of slope period during strong earthquakes. However, NSBM is a simple equivalent-linear sliding method and is limited to provide a simple index for seismic dynamic performance of slopes [35]. Therefore, it is required to identify optimal IM for seismic stability and risk assessment of slopes using a more accurate numerical model for different slopes. To the best of the authors' knowledge, there exists no relevant work for the optimal IM selection of open-pit mine slopes by using nonlinear numerical model and multiple evaluation criteria.

The current study sets out to identify the optimal IM for probabilistic seismic stability assessment of open-pit mine slopes under different mining depths. To this end, actual open-pit slopes with different mining depths are constructed as the reference cases for the numerical investigation. The randomness of input bedrock ground motions and the uncertainty of material properties of the slopes are also considered in this study. A total of 96 ground-motion records and 29 common IMs are selected for testing. Through a series of nonlinear dynamic time-history analyses, the PSDM between IM and the minimum factor of safety (FOS) are constructed. Optimal IMs of the open-pit mine slopes with different mining depths are identified based on the evaluation of five criteria: correlation, efficiency, practicality, proficiency, and sufficiency. Finality, the fragility curves and FOS response hazards of the open-pit mine slopes are generated and discussed by using different IMs. Figure 1 shows the flowchart to identify optimal IMs for probabilistic seismic stability assessment of the open-pit slopes.

2. PSDM and Criteria of Optimal IM Identification

2.1. PSDM Formulation. A PSDM based on PSDA describes the conditional probability of engineering demand parameter (EDP) (e.g., minimum factor of safety (FOS), maximum displacement response, maximum acceleration response,

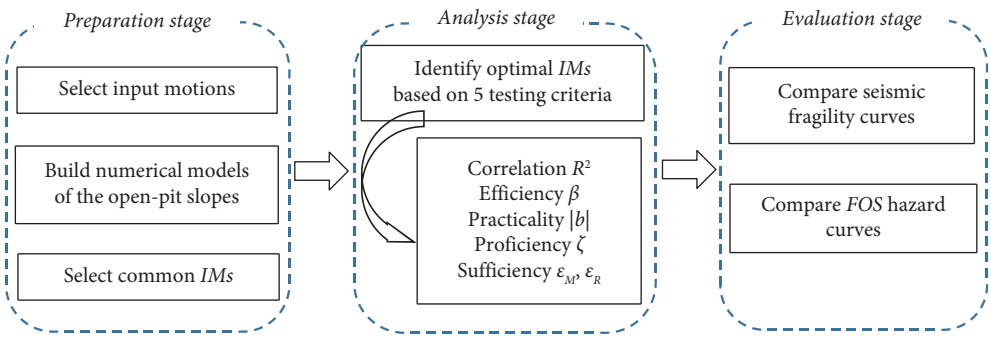

Figure 1: Flowchart of the analytical framework to identify the optimal IMs for the open-pit slopes.

and maximum shear stain) of an open-pit mine slope reaching or exceeding a certain edp level for a given seismic IM level. A log-normal distribution is often used to quantify such conditional probability $P(EDP \geq edp|IM)$ [36, 37], as expressed in the following equation:

$$P(EDP \geq edp|IM) = 1 - \Phi\left(\frac{\ln(edp) - \ln\left(\mu_{EDP|IM}\right)}{\beta_{EDP|IM}}\right), \tag{1}$$

where $\Phi(\cdot)$ denotes the standard normal cumulative distribution function, $\mu_{EDP|IM}$ is the median seismic demand of the open-pit slope for a given IM level, and $\beta_{EDP|IM}$ is the logarithmic standard deviation of the seismic demand conditioned on the given IM level.

The median seismic demand $\mu_{EDP|IM}$ of the open-pit slope is usually assumed to follow a power-law function against the IM, as shown in the following equation:

$$\mu_{EDP|IM} = a \cdot IM^b, \tag{2}$$

where a and b are the regression coefficients from nonlinear time-history analyses of the open-pit slope.

For simplicity, the power-law function can be rearranged to natural logarithmic space which describes a linear expression of $In(\mu_{EDP|IM})$ with regard to In (IM), as follows:

$$In\left(\mu_{EDP|IM}\right) = In(a) + b \times In(IM), \tag{3}$$

where $In(a)$ and b are the vertical intercept and the slope factor, respectively.

It is worth noting that the power-law function of equation (2) are not the only possible models for predicting the seismic demand of slopes conditioned on a given IM value. Other models, such as quadratic function [38] and artificial neural networks [39, 40], can also be used to provide the relation between EDP and IM.

The uncertainty of seismic demand $\beta_{EDP|IM}$ is assumed constant with respect to IM and can be approximately estimated by calculating the dispersion of the seismic demands of the slope around the predicted one using the following equation:

$$\beta_{EDP|IM} \cong \sqrt{\frac{\sum_{i=1}^{N}\left[\ln(edp_i) - \ln\left(\mu_{EDP|IM}\right)\right]^2}{N-2}}, \tag{4}$$

where edp_i is the ith calculated seismic demand of the open-pit slope subjected to the ith ground-motion record, and N is the total number of nonlinear time-history analyses for a suite of selected ground-motion records.

From the above-given functions, the first priority for developing a PSDM of the open-pit slope is to determine an optimal seismic IM for the specified EDP (such as FOS). An optimal IM can effectively improve the ability of constructed PSDM to estimate the seismic responses of the open-pit slope. However, the identification of an optimal IM still is a challenging for open-pit mine slopes. In the current study, the optimal IMs for open-pit slopes are identified based on the five criteria in the below section.

2.2. Criteria of Optimal IM Identification. Five testing criteria, which have been typically utilized in other literature for different engineering structures [41], are adopted to identify optimal IMs in this study. They are correlation [42], efficiency [42], practicality [43], proficiency [44], and sufficiency [45]. Each of these testing measures would be briefly explained below.

2.2.1. Correlation. The correlation criterion reflects the goodness of fit of the empirical regression model of equation (3) to predict the seismic responses of the open-pit slope. The correlation of an IM can be measured by the adjusted coefficient of determination R^2, which is a popular statistical indicator for correlation between variables. The value is less than or equal to 1. A larger R^2 value can strongly implies a better correction between the specified EDP and the given IM.

2.2.2. Efficiency. Efficiency of an IM determines the level of variability or dispersion of the calculated seismic responses around the regression model for a given IM. For this study, the conditional standard deviation $\beta_{EDP|IM}$ obtained from the logarithmic linear regression is used to quantify the efficiency of a candidate IM, as shown in equation (4). Due to being inversely proportional to the efficiency, a more efficient IM would lead to a lower value of $\beta_{EDP|IM}$ and indicates a less dispersion around the predicted values from equation (3). In general, a PSDM with dispersion $\beta_{EDP|IM}$ less than 0.30 can be regarded as satisfactory [30].

2.2.3. Practicality. Practicality represents the dependency of the EDP of the open-pit slope against an IM. For the conventional linear regression, practicality can be quantified by the absolute value of slope factor $|b|$ of regression model in equation (3). The regression model for an IM having higher $|b|$ value demonstrates that the IM is significantly dependent on the specified EDP. Such an IM is more practical. Conversely, the contribution of an IM for the prediction of the specified EDP is negligible if the absolute value of slope factor $|b|$ closes to zero. That is, a lower absolute value of slope factor shows a less practical IM.

2.2.4. Proficiency. Proficiency is a composite indicator that can measure the simultaneous effect of both efficiency and practicality. The proficiency index is also referred as modified dispersion ζ, which can simplify the optimal IM identification in terms of the highest practicality and lowest dispersion. In general, a lower ζ value indicates a more proficient IM. The proficiency index can be calculated from the following equation:

$$\zeta = \frac{\beta_{EDP|IM}}{|b|}, \tag{5}$$

where $\beta_{EDP|IM}$ is the standard deviation of regression model and $|b|$ is the absolute value of slope factor.

2.2.5. Sufficiency. Sufficiency suggests the statistical dependency between a candidate IM of ground motions and some seismological parameters such as magnitude (M) and source-to-site distance (R). For a sufficient IM, the probability distribution of the seismic demands of the open-pit slope should be conditionally independent of such seismological parameters [46], as shown in the following equation:

$$P[EDP \geq edp|IM] \cong P[EDP \geq edp|IM, M, R]. \tag{6}$$

The sufficiency criterion can be quantified by p value [47, 48], which indicates the probability of rejecting the null hypothesis (the slope factor b of linear regression model between the calculated EDP residuals and seismological parameters equals zero) in variance analysis. A higher p value denotes the candidate IM is sufficient. Significance levels of 5% ($p = 0.05$), which is frequently used in previous researches and practices, is adopted as the threshold for distinguishing the sufficiency of an IM herein. In other words, a candidate IM which leads to $p < 0.05$ would be considered as an insufficient IM. Numerically, the p value can be obtained from one-parameter linear regression analysis of residuals $\varepsilon_{EDP|IM}$ between the calculated seismic demand and the predicted value of a slope from equation (3) with respect to M or R, as shown in the following equation:

$$\begin{aligned} \varepsilon_{EDP|IM} &= a_M + b_M \times (M), \\ \varepsilon_{EDP|IM} &= a_R + b_R \times (R). \end{aligned} \tag{7}$$

A brief illustration of efficiency, practicality, and sufficiency of an IM against FOS is depicted in Figure 2. It is observed that the FOS response of the slope decreased with the increase of IM levels. IM_1, which has lower β and higher $|b|$ value, is more efficient and practical; whereas, IM_2 is the opposite. To the FOS residuals with respect to a seismological parameter, the bias is obvious and has a p value less than the significance level 0.05 when IM_2 is used. Consequently, IM_2 is regarded as insufficient. Therefore, in order to identify optimal IMs, the abovementioned parameters such as coefficient of determination R^2, dispersion β, absolute value of slope factor $|b|$, and p-values need to be calculated and compared in regression analysis.

3. Slope Description and Numerical Modeling

3.1. Open-Pit Slope Description. The case-study slope is a typical open-pit mine slope that is located at the Kyisintaung (K) mine in the south of Sagaing Province, Myanmar. The K mine is a porphyry copper mine with a length of 750~980 m and a width of 550~700 m. It came on stream in 2015. Based on the location, lithology, and design height, the K mine is divided into four engineering geological areas, namely, A, B, C, and D, which represent the east, south, west, and north areas, respectively. Maximum slope design height in open boundary of A, B, C, and D area are 420 m, 460 m, 400 m, and 290 m, respectively. The schematic diagram of the open-pit mine is presented in Figure 3. The mining design parameters are specified as follows: step height is set to 10 m except for the one of final parallel section, which is 20 m. Widths of safety platform and cleaning platform are 8 m and 16 m, respectively. Width of haulage road is 16 m for one lane, and 21 m for two lanes. Minimum design radius and maximum gradient of haulage road are 20 m and 8%, respectively. Control angles of final slopes are area $A \leq 40^\circ$, area $B \leq 41^\circ$, and area $C \leq 40^\circ$. More details about the K mine can be available in the related literature [49, 50].

3.2. Numerical Modeling. To identify the optimal IMs for PSDM of the open-pit slopes under different mining depths, the $A1$ engineering geological profile in area A is taken as the case-study slope (see Figure 3(c)). The maximum design height and angle of the $A1$ slope profile are 310 m and 39.4°, respectively.

Based on the geological parameters of the $A1$ profile, four two-dimensional numerical models with different mining depths are constructed by the finite element software ABAQUS. The slope angles are kept constant at 39.4°, and the mining depths of the slope are set as 50 m, 100 m, 200 m, and 300 m, respectively. The range of the rock mass in the horizontal front of slope foot is taken as 1.5 times of the slope height (H) and the rock mass range behind the horizontal edge of slope top is 2.5H. The bottom boundary of a slope along vertical direction is 2.0H. The slope models are discretized using 4-node reduced integration elements (CPE4R) for the rock masses. To ensure the accuracy of the computation, the finite element size of the rock masses is set to 0.5 m. When performing the static analysis for gravity, the fixed constraints are imposed on the bottom and side boundaries of the models. Considering the radiation

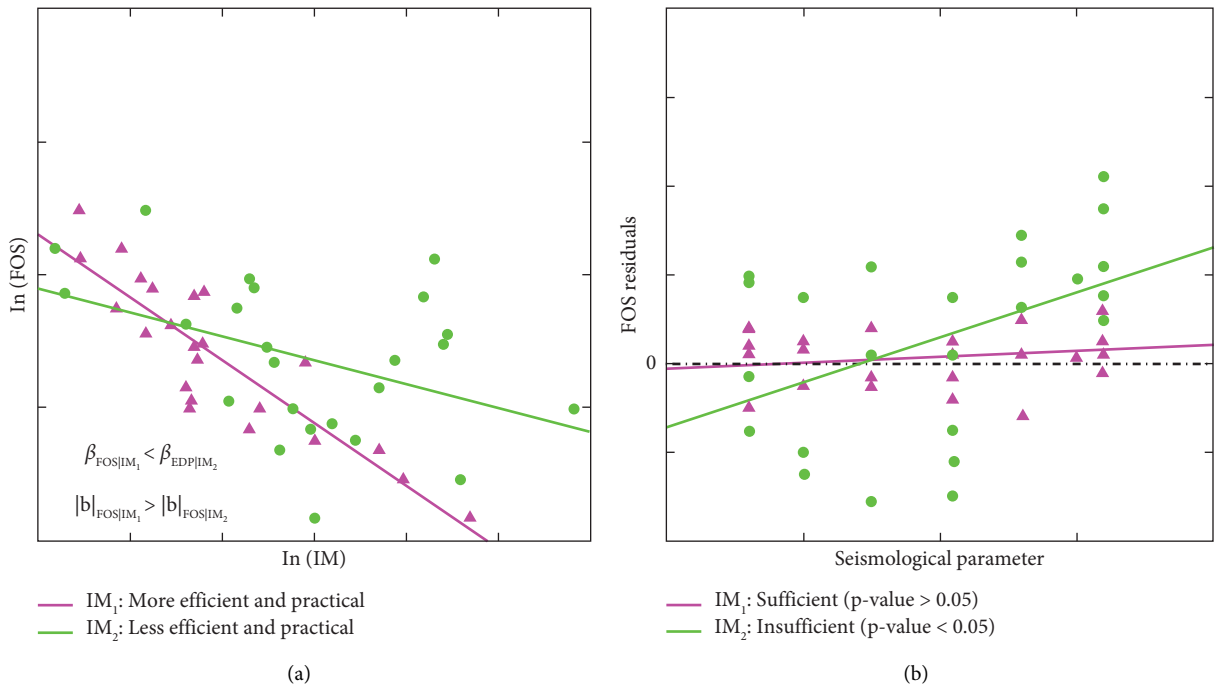

Figure 2: Illustration of (a) IM efficiency and practical and (b) IM sufficiency.

damping effect of seismic waves, the viscous boundary is applied at the bottom, while the parasitic boundary has been adopted for the left and right sides when the dynamic seismic analyses are performed. The rock physical and mechanical properties of the open-pit slope along $A1$ profile are listed in Table 1. The nonlinear dynamic behavior of the rock materials is simulated using the Martin–Davidenkov model proposed by Martin and Seed [51] that can be calculated using the following equation:

$$\begin{cases} \tau(\gamma) = G \cdot \gamma = G_{\max} \cdot \gamma [1 - H(\gamma)], \\ H(\gamma) = \left\{ \dfrac{(\gamma/\gamma_0)^{2b}}{1 + (\gamma/\gamma_0)^{2b}} \right\}^a, \end{cases} \tag{8}$$

where the $\tau(\gamma)$ denotes the shear stress; G and $G_{\max}$ are the shear modulus and the maximum shear modulus, respectively; and γ is the shear strain. a, b, and γ_0 are the fitting parameters.

The schematic diagram of numerical modeling of the open-pit mine slope case along the $A1$ profile is depicted in Figure 4. According to the eigenvalue analyses using Lanczos iteration method, the first mode periods of the four slopes are 0.25 s, 0.68 s, 1.42 s, and 1.94 s, respectively. Based on the wave propagation theory [28], the input motion at the base boundary is roughly equal to half of the surface motion at bedrock outcrop. Therefore, the amplitude of the selected records in Section 4.1 are first scaled by 0.5 and then used as the input base motions for the numerical analyses. Due to large span of the slopes, the spatial variation of input motions at the bedrock boundary should be considered. Spatial variations of input bedrock motions mainly include wave passage and wave scattering. In contrast, the wave-passage effect has more influence on the slope responses. It is assumed that the waveform of input motions at different locations of the bedrock boundary is same. The propagation delay time along the horizontal direction from the middle of the bedrock boundary to other input points are calculated by the following equation:

$$\Delta t = \frac{d}{v}, \tag{9}$$

where d is the distance between each input point and the middle of the bedrock boundary and v is the velocity of seismic wave, which is set to 1000 m/s.

3.3. Uncertainty Modeling. In the derivation of PSDM and fragility function, a probabilistic approach is used owing to the uncertainties in seismic response and seismic capacity of the open-pit slopes. The uncertainties are often classified into two groups: aleatoric uncertainty (inherent randomness) and epistemic uncertainty (lack of knowledge). In addition to the randomness of the ground motion considered in Section 4.1, the variation of modeling parameters of slopes should also be included, which is often neglected due to the lack of knowledge regarding material properties. Many uncertain modeling parameters of slopes are adopted in previously studies. In this study, three uncertain modeling parameters of the slopes are adopted including rock elastic modulus (E), internal friction angle (φ), and cohesive (c). The correlations between these modeling parameters are ignored because of the lack of relevant studies. Based on the results of previous studies [21, 52–54], Table 2 presents the probability distribution types of three modeling parameters and coefficients of variation (COV). Normal distribution is specified for the three modeling parameters in the dynamic

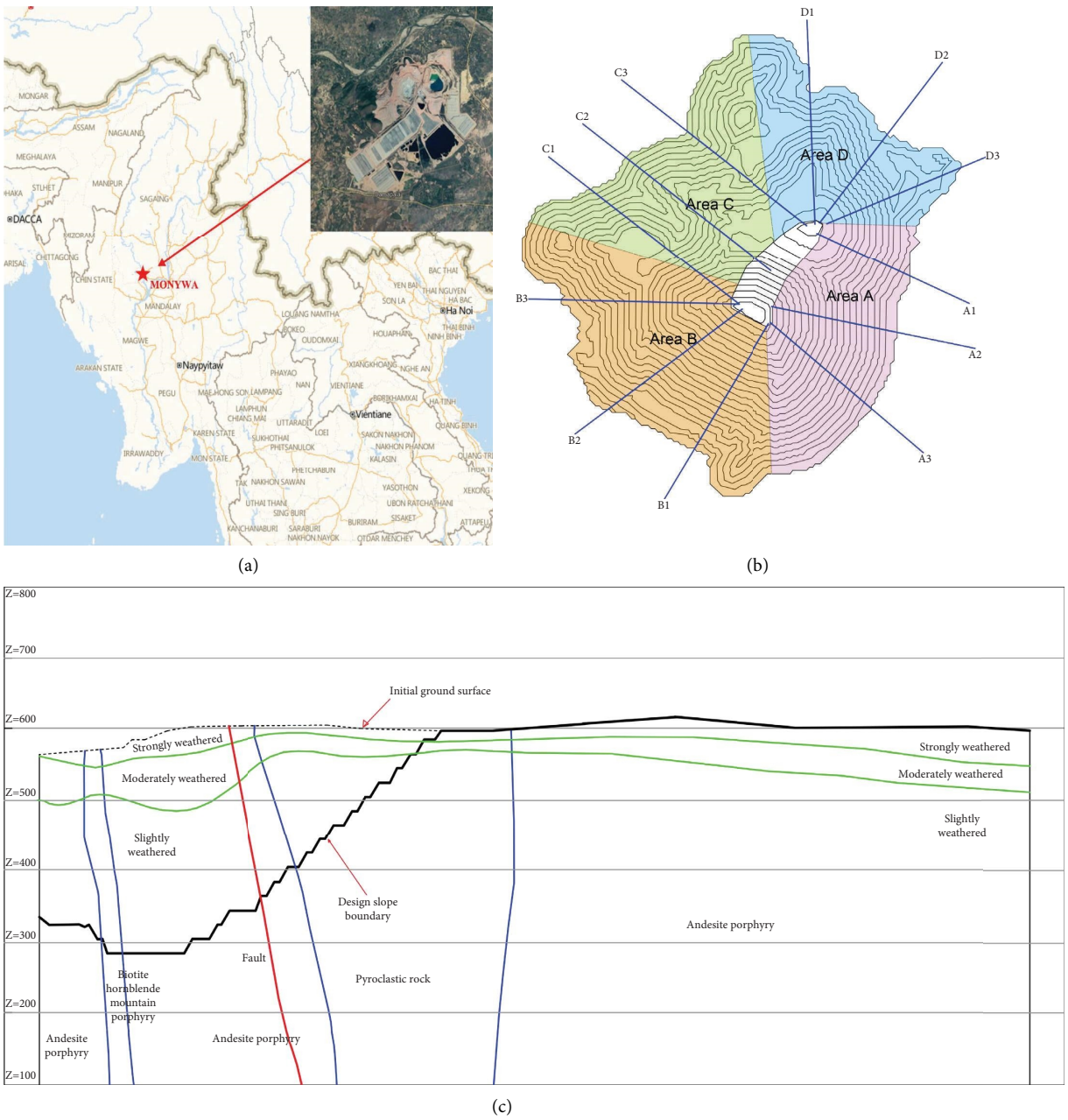

Figure 3: Illustration of the *K*open-pit mine in Myanmar. (a) Location. (b) Engineering geological division. (c) *A*1 engineering geological profile.

response analyses of slopes. It is worth noting that the three material parameters for the slope modeling are first randomly generated according to the probability distribution of Table 2 before the dynamic response analyses of slopes are implemented under earthquake records.

3.4. Definition of Damage States. It is essential to define a set of various damage states, corresponding seismic performance levels, and damage indices for subsequent fragility analyses of the open-pit slopes in Section 5.7. The minimum factor of safety (FOS), which has been widely adopted in most seismic design codes to evaluate seismic performance and dynamic stability of slopes, is used as the representative EDP of slopes in this study. Significantly, the requirements for FOS of slopes are different in various codes. For example, the required FOS varies from 1.0 to 1.4 for different safety levels of slopes in Eurocode 8 [55]. To the code for building slope engineering of China [56], the acceptable FOS of slope stability for three importance grades are 1.05, 1.10, and 1.15, respectively. This study adopted five damage states proposed by Lagaros for seismic fragility analyses of open-pit slopes [21]. Five damage states includes: optimal (DS_1), sufficient (DS_2), moderate (DS_3), minor (DS_4), and unacceptable (DS_5). The corresponding relative safety margins and the range of FOS damage indices are presented in Table 3.

Table 1: The rock physical and mechanical properties of the open mining slope along $A1$ profile.

Rock types	Density (kg/m^3)	Elastic modulus (MPa)	Poisson ratio	Internal friction angle (°)	Cohesion (MPa)
Strongly weathered andesite porphyry	2230	241.83	0.30	24	0.16
Moderately weathered andesite porphyry	2390	1561.44	0.30	32	0.25
Slightly weathered andesite porphyry	2580	3587.58	0.22	37	0.76
Strongly weathered pyroclastic rock	2150	284.52	0.29	25	0.17
Moderately weathered pyroclastic rock	2260	1060.40	0.23	30	0.20
Slightly weathered pyroclastic rock	2430	4062.90	0.29	36	0.67
Moderately weathered biotite hornblende mountain porphyry	2560	2953.59	0.25	34	0.60
Slightly weathered biotite hornblende mountain porphyry	2640	7884.14	0.22	39	1.10

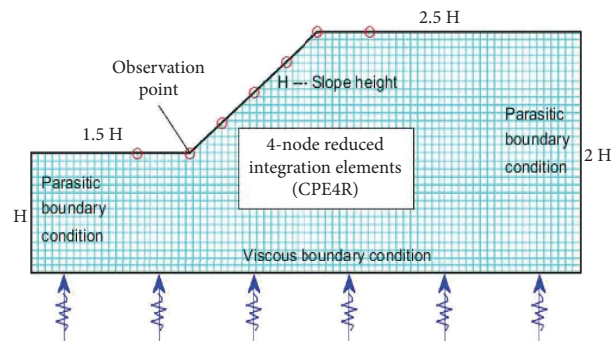

Figure 4: Schematic diagram of numerical modeling of the open-pit mine slope case along the $A1$ profile.

Table 2: Distribution characteristics of slope modeling parameters.

No.	Modeling parameters	Probability distribution	Coefficients of variation (COV)
1	Rock elastic modulus	Normal	0.15
2	Internal friction angle	Normal	0.10
3	Cohesive	Normal	0.10

Table 3: Adopted damage states for open-pit mine slopes in terms of FOS.

Damage states	DS_1 (optimal)	DS_2 (sufficient)	DS_3 (moderate)	DS_4 (minor)	DS_5 (unacceptable)
Relative safety margins	Very high	High	Moderate	Low	None
Range of FOS	>2.0	1.4~2.0	1.25~1.4	1.0~1.25	<1.0

4. Records and Intensity Measures Selection

4.1. Ground-Motion Record Selection. Given the uncertainty of input bedrock seismic motions, a suite of actual records from different significant earthquake events are required for nonlinear seismic response analyses of the open-pit slopes. Different studies may adopt different criteria to select input bedrock motions. Site-specific matching criteria allow for ground-motion selection based on spectral compatibility with a target probability of exceedance level. However, this method is only suitable for estimating the slope responses with a certain probability of exceedance level. Therefore, the input motions selected in this study are not limited to a certain probability of exceedance level and takes into account the contributions of various significant earthquakes for the slope sites [57]. For this study, 4 bins, each containing 12 pairs of horizontal ground-motion records, are collected from the NGA-West2 database developed by the Pacific Earthquake Engineering Research Center [58]. The database provides a large number of strong motion records in worldwide active tectonic regimes, as well as source parameters, distance measures, site conditions, etc. The critical point between large-magnitude (LM) and the small-magnitude (SM) is set as $Mw = 6.5$. Records with $R > 30$ km are grouped into large-distance (LR) bin, and those with $R \leq 30$ km are grouped into small-distance (SR) bin. The details of the selection criteria of actual records are presented as follows:

(i) Earthquake magnitude (M) and source-to-site distance (R) of the selected records should approximately match the M and R of the potential seismic sources around the open-pit slope site.

(ii) To eliminate structural effects, the observation instruments are located on the free-field or at the lowest level of low-rise structures.

(iii) V_{S30} (average shear-wave velocity in the uppermost 30 m) of the observation station is larger than 500 m/s, roughly corresponding to rock site or very dense soils on the NEHRP soil-type$C$ or B.

(iv) Velocity pulse-like records due to near-fault rupture directivity or fling-step effects are excluded. Velocity pulse-like records often exhibit larger amplitudes and shorter durations compared with the general ground motions. However, this issue is beyond the scope of this study.

(v) Aftershock records are excluded.

Two horizontal components at the same station are assumed to be independent, resulting in a total of 96 horizontal motions are adopted as the input bedrock motions for nonlinear time-history analyses of the open-pit slopes. The detailed characteristics of selected records are listed in Table 4. The distribution of selected motions covers a wide range of magnitudes between 5.99 and 7.62, the rupture distance (R_{rup}) up to above 66 km, and the peak ground acceleration (PGA) of the 96 records range from 0.05 and 1.43 g, as illustrated in Figures 5(a) and 5(b). In addition, the individual and median spectral accelerations of the selected 96 motions are shown in Figure 5(c).

4.2. Candidate IMs Selection. An seismic IM can reflect and quantify one or more key characteristics of a nonstationary seismic motion in a simple and measurable form. These characteristics include amplitude, frequency content, duration, and energy distribution of a seismic motion, which are significantly correlated with structural responses. In general, a perfect IM has the ability to obtain all key features of a seismic motion and can accurately predict the seismic response and dynamic stability of the open-pit slope. However, due to the inherent nonstationary of a seismic motion in time and frequency domain, it is very difficult to define a perfect IM that can quantify all significant seismic features [59]. Therefore, it is necessary to investigate the common IMs to determine the optimal IM for the development of PSDM of the open-pit slope. For this study, 29 common IMs are chosen as the candidate IMs, as listed in Table 5. According to their definitions, the 29 IMs can be categorized roughly into four groups: (1) IMs that are related to acceleration time history (e.g., PGA and CAV); (2) IMs that are related to velocity time history (e.g., PGV and VSI); (3) IMs that are related to displacement time history (e.g., PGD and D_{RMS}); and (4) *IMs* that are related to the duration (e.g., D_{5-95}). One also may find more detailed explanations on these candidate IMs in related references [33, 34].

4.3. FOS Time-History Responses. There are many definitions of the factor of safety FOS for slopes. Considering the output results of the FEM analysis and physical implications, FOS is defined as the ratio of the antislide force and the slide force on a certain slip surface. It can be calculated from the following equation:

$$FOS = \frac{\sum (c_i + \sigma_i \tan \phi_i) l_i}{\sum \tau_i l_i}, \tag{10}$$

where l_i, σ_i, and τ_i are the geometric length, normal stress, and shear stress of segment i on a slip surface, respectively. c_i, and ϕ_i are the corresponding cohesive and internal friction angle.

The calculation steps of the dynamic FOS time history of a slope when subjected a seismic record are as follows [60]: (1) the stress field at each time step is calculated through performing the FEM dynamic response analyses of a slope. (2) A number of potential slip surfaces are generated for a time step. (3) The FOS are calculated by equation (10) for each potential slip surface at this time step and the minimum FOS are defined as the instantaneous FOS at this time step. (4) Repeat steps (2) and (3) for each time step and the whole dynamic FOS response time history of a slope case can be captured. Nonlinear time-history analyses of the open-pit slopes with different mining depths are performed under 96 input ground motions. Figure 6 presents the FOS time-history responses of the four slopes under the 2007 Chuetsu-oki earthquake record in Iizuna Imokawa station. It can be seen that the FOS responses of the slopes under different mining depths are obviously different. The slope with a mining depth of 100 m has the worst stability than others, and its minimum FOS is 1.777. This may partly be due to the fact that the natural period of this slope is closest to the predominant period (0.71 s) of this seismic record. In contrast, the natural period of the slope with a mining depth of 300 m, which has the minimum FOS of 2.716, is far from the predominant period of the seismic record and is most stability among the four slopes.

5. Results and Discussion

To evaluate the optimality of the candidate IMs with respect to FOS, the PSDMs between all candidate IMs and FOS are constructed based on the regression results of time-history analyses of the slope cases. The optimal IMs are identified by correlation, efficiency, practicality, proficiency, and sufficiency. Subsequently, seismic fragility curves and FOS response hazard curves of the open-pit slopes are compared using different IMs. Before that, the PSDMs of FOS against PGA are presented to illustrate the influence of ground-motion characteristics on the FOS responses of the slopes. Figure 7 plots the PSDMs of the four slopes with respect to PGA on the logarithmic scale. It is noted that the correlation between PGA and FOS responses of the four slopes is low, and the highest correlation coefficient is only 0.648. The dispersion of PSDM for the slope with a mining depth of 300 m is the highest, reaching 0.424. It shows that PGA is less effective to predict the FOS of this slope. It is also observed that there is little difference for the absolute value of slope factor $|b|$ in all slope cases. These results suggest that PGA is not an appropriate IM for accurately predicting the seismic FOS of open-pit slopes. Therefore, the selection of the optimal IM from lots of common IMs is of great significance for the development of PSDM of open-pit slope.

5.1. Correlation Comparison. The correlation criterion can reflect the goodness of fit of PSDM to predict the seismic FOS of a slope using a candidate IM. Figure 8 compares the calculated correlation coefficients (R^2) between FOS and 29 candidate IMs for the open-pit slopes under different mining depths.

It is clear that the most correlated IMs vary with different mining depths. SMV exhibits the most strongest correlation with the FOS for the slope with a mining depth of 50 m, followed by PGV and HI. The corresponding values of R^2 are 0.887, 0.866, and 0.853, respectively. Meanwhile, the weakest correlated IM is FR2, followed by D_{5_95}, and FR1. Their values of R^2 are 0.006, 0.060, and 0.266, respectively. For the slope with a mining depth of 100 m, Sv ($1.5T_1$) is the most correlated IM, followed by VSI and HI. The correlation coefficients for the three most correlated IMs are 0.869, 0.848, and 0.805, respectively. Interestingly, FR2 and D_{5_95} are once again the two least correlated IMs. This finding is well in line with the results of the slope case with a mining depth of 50 m. In the case of the slope with a mining depth of 200 m, three most correlated IMs are VSI, SMV, and HI, and their values of R^2 are 0.864, 0.805, and 0.790, respectively. Whereas the lowest correlated IM for FOS is FR2, followed by D_{5_95}. Their corresponding correlation coefficients are 0.009 and 0.012, respectively. Furthermore, VSI is once again the most correlated IM for the slope with a mining depth of 300 m. HI and SMV are other two following highly correlated IMs. The correlation coefficients for three IMs are 0.810, 0.809, and

Table 4: Detailed characteristics of selected ground-motion records.

Bins	Events	Year	Stations	M_w	R_{rup} (km)	V_{S30} (m/s)	PGA* (g)
L	Loma Prieta	1989	LGPC	6.93	3.88	595	0.59
M	Northridge-01	1994	Beverly hills—12520 Mulhol	6.69	18.36	546	0.54
S	Northridge-01	1994	Simi valley—Katherine rd	6.69	13.42	557	0.64
	Chi-Chi, Taiwan	1999	CHY028	7.62	3.12	543	0.77
	Chi-Chi, Taiwan	1999	TCU071	7.62	5.80	625	0.59
	Chi-Chi, Taiwan	1999	TCU084	7.62	11.48	665	0.74
	Manjil, Iran	1990	Abbar	7.37	12.55	724	0.52
R	Chuetsu-oki	2007	Joetsu Oshimaku Oka	6.8	22.48	610	0.62
	Chuetsu-oki	2007	KCT	6.8	20.03	561	0.55
	Chuetsu-oki	2007	KNI	6.8	12.63	655	0.86
	Iwate	2008	IWTH25	6.9	4.80	506	1.35
	Iwate	2008	Kurihara city	6.9	12.85	512	0.59
L	Chi-Chi, Taiwan	1999	ILA067	7.62	38.82	665	0.21
M	Tottori, Japan	2000	OKYH10	6.61	46.37	554	0.22
L	Tottori, Japan	2000	SMNH12	6.61	45.07	590	0.25
	Chuetsu-oki	2007	Joetsu, Aramaki district	6.8	32.54	606	0.23
	Chuetsu-oki	2007	Tokamachi Chitosecho	6.8	30.65	640	0.22
	Chuetsu-oki	2007	Iizuna Imokawa	6.8	66.44	591	0.57
	Chuetsu-oki	2007	Toyotsu Nakano	6.8	63.54	562	0.23
R	Iwate	2008	IWT009	6.9	33.28	517	0.25
	Iwate	2008	IWTH27	6.9	43.59	670	0.23
	Iwate	2008	MYG002	6.9	57.3	527	0.30
	Iwate	2008	Miyagi great village	6.9	41.13	531	0.20
	Iwate	2008	Okura, Aobaku, Sendai	6.9	53.88	640	0.24
S	Parkfield	1966	Temblor pre-1969	6.19	15.96	528	0.29
M	Coalinga-01	1983	Slack Canyon	6.36	27.46	648	0.16
S	Chalfant valley-02	1986	Bishop-Paradise lodge	6.19	18.31	585	0.15
	Whittier narrows-01	1987	Alhambra-Fremont school	5.99	14.66	550	0.31
	Whittier narrows-01	1987	Big Tujunga, Angeles Nat F	5.99	28.5	550	0.17
	Whittier narrows-01	1987	Mt Wilson-CIT Seis Sta	5.99	22.73	680	0.16
	Parkfield-02, CA	2004	PARKFIELD-DONNA LEE	6	4.93	657	0.34
R	Parkfield-02, CA	2004	Parkfield-Cholame 2E	6	4.08	523	0.48
	Parkfield-02, CA	2004	Parkfield-fault zone 11	6	4	542	0.83
	Parkfield-02, CA	2004	Parkfield-gold hill 3W	6	5.41	511	0.60
	Parkfield-02, CA	2004	Parkfield-stone corral 2E	6	5.80	566	0.19
	Christchurch, NZ	2011	LPCC	6.20	6.12	650	0.93
S	Coalinga-01	1983	Parkfield-gold hill 3W	6.36	39.1	511	0.12
M	Coalinga-01	1983	Parkfield-stone corral 2E	6.36	36.4	566	0.09
L	Coalinga-01	1983	Parkfield-stone corral 3E	6.36	34	565	0.10

Table 4: Continued.

Bins	Events	Year	Stations	M_w	R_{rup} (km)	V_{S30} (m/s)	PGA* (g)
	N. palm springs	1986	Anza-red mountain	6.06	38.4	680	0.09
	N. palm springs	1986	Anza-tule canyon	6.06	52.1	531	0.16
	N. palm springs	1986	Santa sosa mountain	6.06	39.1	679	0.07
	Whittier narrows-01	1987	Mill Creek, Angeles Nat for	5.99	36.8	570	0.07
R	Whittier narrows-01	1987	Pacoima kagel canyon	5.99	36.1	508	0.14
	Whittier narrows-01	1987	Vasquez rocks park	5.99	50.4	996	0.05
	Big bear-01	1992	Silent valley-poppet flat	6.46	35.4	659	0.12
	Big bear-01	1992	Snow creek	6.46	38.1	523	0.09
	Christchurch, NZ	2011	SCAC	6.2	66.5	561	0.10

*The PGA values are the median of orientation independent amplitudes (RotD50) from the PEER NGA-West2 database flat file.

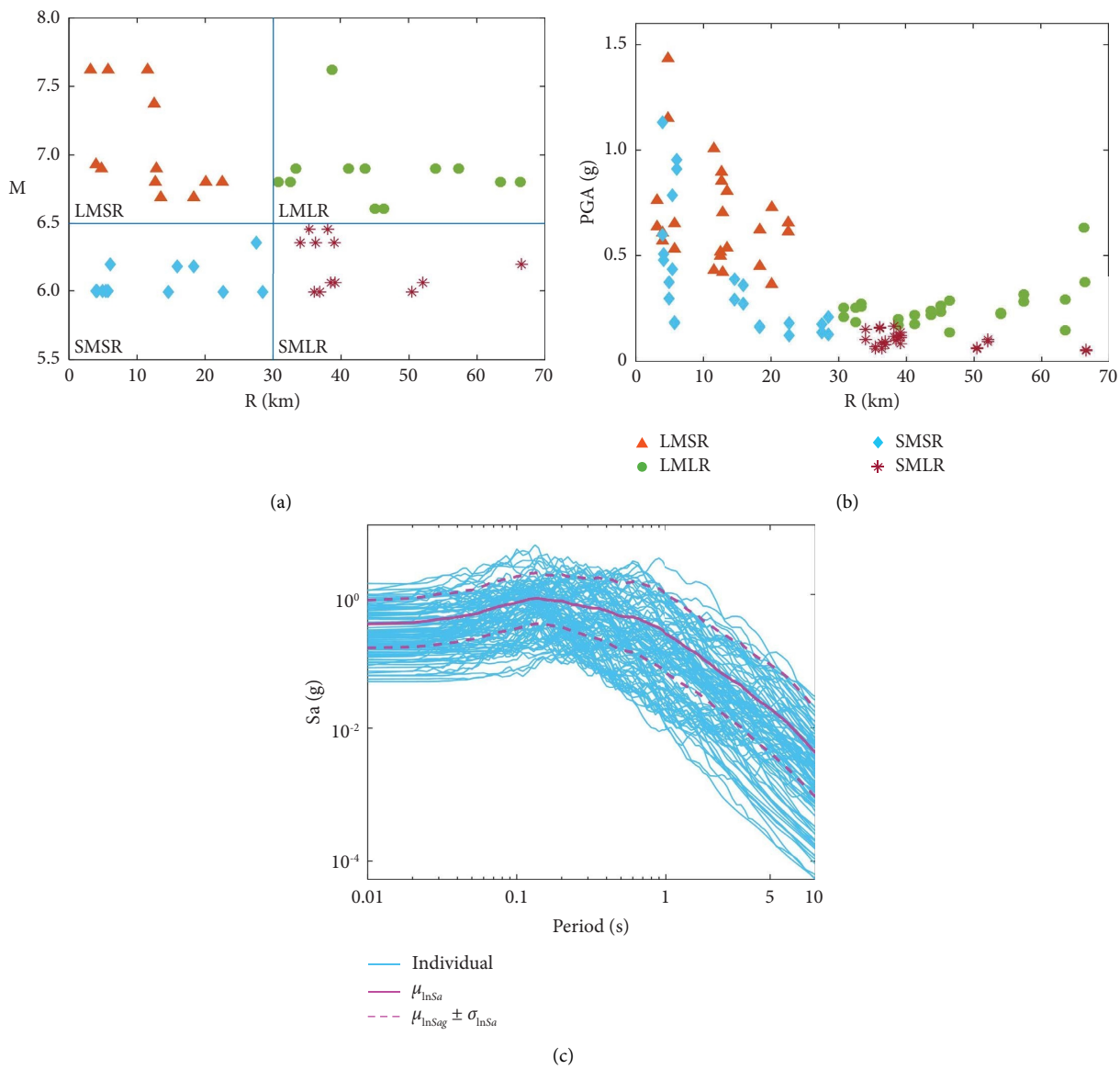

Figure 5: Characteristics of selected ground-motion records: (a) *M-R* distribution, (b) PGA-*R* distribution, and (c) spectral acceleration with 5% damping ratio.

0.807, respectively. FR2 and D_{5_95} are two weakest correlated IM against FOS with smaller values of R^2. Compared with PGA and Sa (T_1), PGV is more correlated with FOS responses of the slopes among three most commonly used IMs.

5.2. Efficiency Comparison. The efficiency criterion reflects the level of variability of the calculated FOS around the regression model. The results of the efficiency between FOS and 29 candidate IMs for the open-pit slopes under different mining depths are summarized in Figure 9.

For the slope with a mining depth of 50 m, SMV, PGV, and VSI are three most efficient IMs because of less dispersion for FOS. The β values for them are 0.061, 0.118, and 0.169, respectively. The maximum dispersion is FR2, i.e., 0.892, indicating the lowest efficiency. It is followed by D_{5_95} and PGD. Their corresponding dispersion are 0.880, and 0.685, respectively, which are slightly lower than the value of FR2. In the case of the slope with a mining depth of 100 m, VSI is the most efficient IM with the lowest dispersion of 0.145 and are followed by HI and Sa (T_1), and their β values are 0.177 and 0.190, respectively, which are slightly higher than that of VSI. In contrast, HI, Sv ($1.5T_1$), and PGV are three most efficient IMs for the slope with a mining depth of 200 m, and the corresponding β values are 0.134, 0.237, and 0.249, respectively. Furthermore, for the slope with a mining depth of 300 m, HI is also proved to be the most efficient IM with the smallest standard deviation of 0.150, followed by Sv ($1.5T_1$) and VSI. The β values for the latter IMs are 0.223 and 0.226, respectively. It is noted that FR2, D_{5_95}, and PGD exhibit the worst efficiency when using all slope cases. Moreover, the efficiency of velocity-related IMs is higher than that of acceleration-related IMs and displacement-related IMs.

Table 5: Candidate intensity measures for this study.

No.	Categories	IM	Description	Definition	Units
1	Acceleration-related	PGA	Peak ground acceleration	Max ($\lvert a\ (t)\rvert$)	m/s^2
2		SMA	Sustained maximum acceleration	3rd largest peak in acceleration time history	m/s^2
3		Ia	Arias intensity	$\pi/2g\int_0^{t_D}[a(t)]^2\mathrm{d}t$	m/s
4		CAV	Cumulative absolute velocity	$\int_0^{t_D}\lvert a(t)\rvert^2\mathrm{d}t$	m/s
5		A_{RMS}	Acceleration root-mean-square	$\sqrt{1/t_D\int_0^{t_D}[a(t)]^2\mathrm{d}t}$	m/s^2
6		Ic	Characteristic intensity	$(A_{RMS})^{2/3}\times\sqrt{t_D}$	—
7		EDA	Effective design acceleration	Peak acceleration value remaining after filtering out frequencies beyond 9 Hz	m/s^2
8		A95	A95 parameter	95% acceleration level of total arias intensity	m/s^2
9		Sa (T_1)	Spectral acceleration at T_1	$Sa(T_1,\xi=0.05)$	m/s^2
10		Sa ($1.5T_1$)	Spectral acceleration at $1.5T_1$	$Sa(1.5T_1,\xi=0.05)$	m/s^2
11	ASI	Acceleration spectrum intensity	$\int_{0.1}^{0.5}Sa(T,\xi=0.05)\mathrm{d}T$	m/s	
12	EPA	Effective peak acceleration	$\mathrm{mean}[\int_{0.1}^{0.5}Sa(T,\xi=0.05)\mathrm{d}T]/2.5$	m/s^2	
13		PGV	Peak ground velocity	Max ($\lvert v(t)\rvert$)	m/s
14		SMV	Sustained maximum velocity	3rd largest peak in velocity time history	m/s
15		V_{RMS}	Velocity root-mean-square	$\sqrt{1/t_D\int_0^{t_D}[v(t)]^2\mathrm{d}t}$	m/s
16		SED	Specific energy density	$\int_0^{t_D}[v(t)]^2\mathrm{d}t$	m^2/s
17		FR1	Frequency ratio 1	PGV/PGA	s
18	Velocity-related	Sv (T_1)	Spectral velocity at T_1	$Sv(T_1,\xi=0.05)$	m/s
19		Sv ($1.5T_1$)	Spectral velocity at $1.5T_1$	$Sv(1.5T_1,\xi=0.05)$	m/s
20		VSI	Velocity spectrum intensity	$\int_{0.1}^{2.5}Sv(T,\xi=0.05)\mathrm{d}T$	m
21		EPV	Effective peak velocity	$\mathrm{mean}[\int_{0.8}^{1.2}Sv(T,\xi=0.05)\mathrm{d}T]/2.5$	m/s
22		HI	Housner intensity	$\int_{0.1}^{2.5}PSv(T,\xi=0.05)\mathrm{d}T$	m
23		PGD	Peak ground displacement	Max ($\lvert d(t)\rvert$)	m
24		D_{RMS}	Displacement root-mean-square	$\sqrt{1/t_D\int_0^{t_D}[d(t)]^2\mathrm{d}t}$	m
25	Displacement-related	FR2	Frequency ratio 2	PGD/PGV	s
26		Sd (T_1)	Spectral displacement at T_1	$Sd(T_1,\xi=0.05)$	m
27		Sd ($1.5T_1$)	Spectral displacement at $1.5T_1$	$Sd(1.5T_1,\xi=0.05)$	m
28		DSI	Displacement spectrum intensity	$\int_2^5 Sd(T,\xi=0.05)\mathrm{d}T$	—
29	Duration-related	D_{5-95}	Significant duration	$t_{0.95Ia}-t_{0.05Ia}$	s

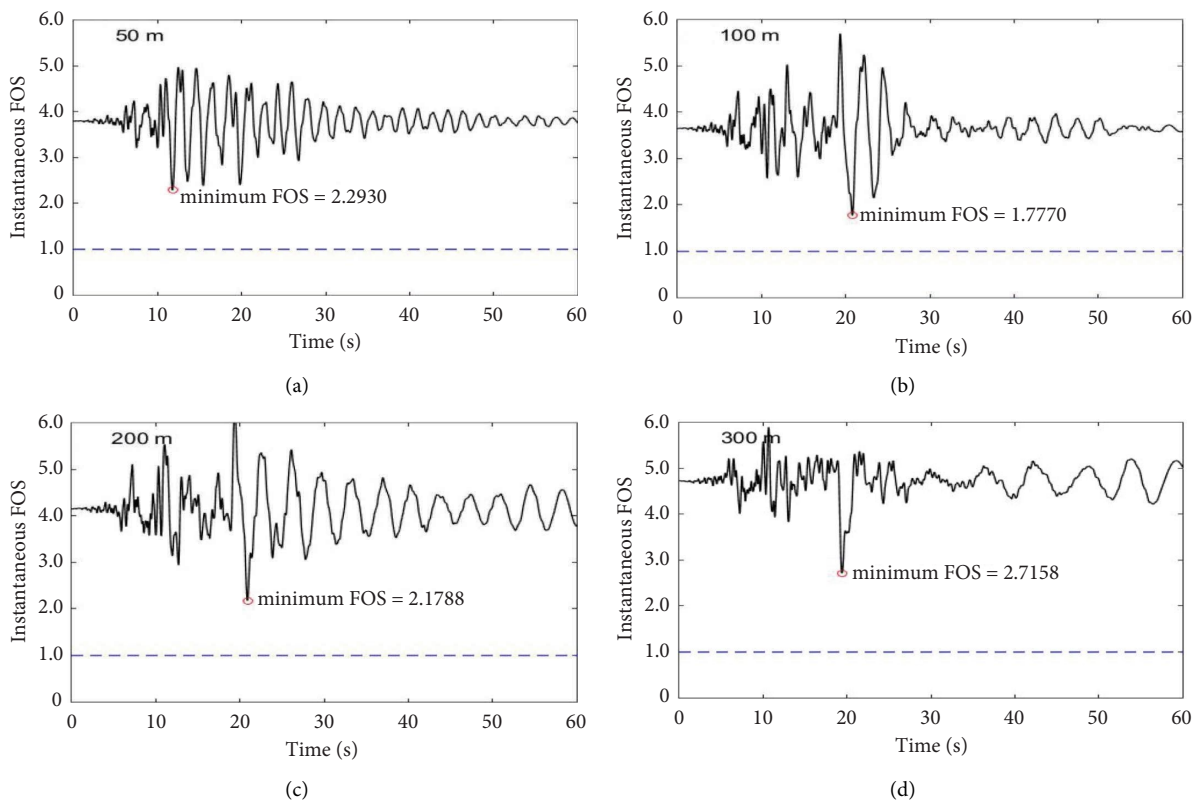

Figure 6: FOS time-history response of the open-pit slopes with different mining depths under the 2007 Chuetsu-oki earthquake record in Iizuna Imokawa station. (a) 50 m. (b) 100 m. (c) 200 m. (d) 300 m.

5.3. Practicality Comparison. Practicality refers to the dependence of the FOS of slopes against the IM and can be represented by the absolute value of regression coefficient $|b|$ in equation (3). A more practical IM shows a larger value of $|b|$, and vice versa. Figure 10 shows the calculated $|b|$ values of each IM-FOS pair for the slopes under four different mining depths.

Figure 10 suggests that FR1, having the maximum $|b|$ values, is the most practical IM for all slope cases with different mining depths, except for the slope of 50 m. ASI, FR1, and CAV are proved to be the three most practical IMs for the slope with a mining depth of 50 m, with the corresponding $|b|$ values equal to 0.425, 0.420, and 0.418, respectively. Meanwhile, FR2 is the least practical IM, which exhibits the minimum $|b|$ value of 0.113 for this slope. SED and D_{5_95} are the following two least practical IMs, with slightly higher $|b|$ value, i.e., 0.157 and 0.184, respectively. For the slope with a mining depth of 100 m, ASI and SMA prove to be the two most practical IMs following FR1, and their corresponding $|b|$ value are 0.441 and 0.448, respectively. D_{5_95} and FR2 are once again two least practical IM, with the $|b|$ values of 0.106 and 0.148, respectively. These similar findings for the least practical IMs are also found for the slopes with higher depths. In contrast, A_{RMS} and ASI are identified as the two most practical IM following FR1 for the slope with a mining depth of 200 m and 300 m, and FR2 and D_{5_95} exhibit the lowest practical.

5.4. Proficiency Comparison. Proficiency ζ describes the composite effect of efficiency and practicality, as shown in equation (5). The results of proficiency analyses of all candidate IMs for the slopes under four different mining depths are compared in Figure 11. For the slope with a mining depth of 50 m, SMV is the most proficient IM due to the corresponding smallest ζ of 0.171, followed by PGV and HI, which have ζ values of 0.394 and 0.574, respectively. FR2 is the less proficient IM, which has the maximum ζ, i.e., 7.879. The next two least proficient IMs are D_{5_95} and PGD, and the ζ values are 4.790 and 3.177, respectively, which are considerably lower than the value for FR2. In case of the slope with a mining depth of 100 m, VSI turns out to be the most proficient IM, followed by PGV and HI. The corresponding ζ values of them are equal to 0.442, 0.513, and 0.540, respectively. On the contrary, D_{5_95} is found to be the less proficient IM having the highest ζ of 9.522. FR2 and PGD are found to be the next three least proficient IMs with slightly lower ζ of 6.896 and 4.137, respectively. Interestingly, these results are also found for the slope of 50 m. For the slope with a mining depth of 200 m, HI is the most proficient IM indicated by the smallest ζ of 0.441 compared to other candidate IMs. PGV and Sv ($1.5T_1$) are next two most proficient *IMs* with the ζ values of 0.624 and 0.650, respectively. D_{5_95} is the least proficient IM, followed by FR2 and PGD with corresponding ζ values of 10.099, 7.357, and 3.696, respectively. Furthermore, HI, Sv ($1.5T_1$), and *VSI* are

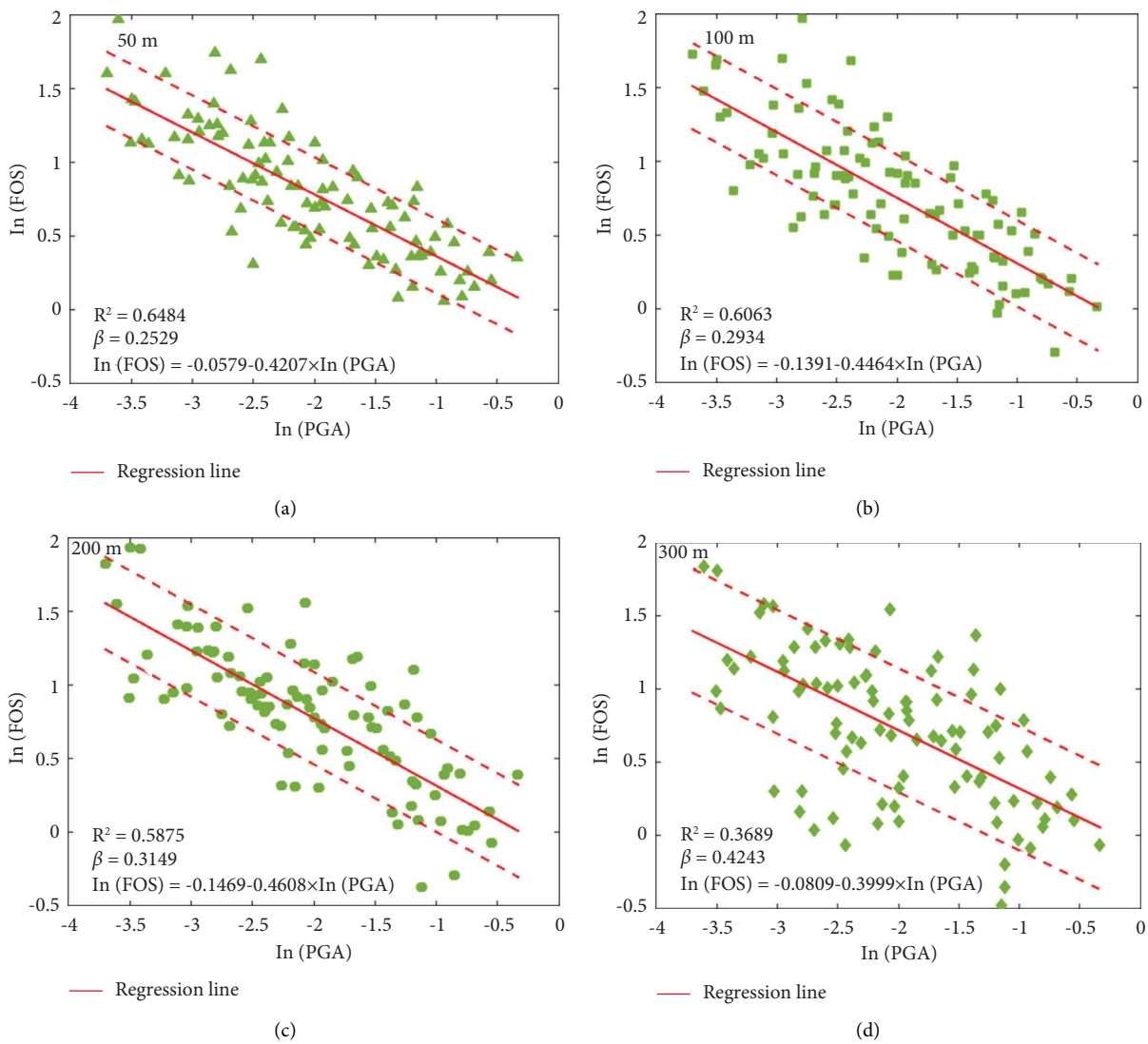

Figure 7: PSDM of FOS with respect to PGA for the open-pit slopes with different mining depths. (a) 50 m. (b) 100 m. (c) 200 m. (d) 300 m.

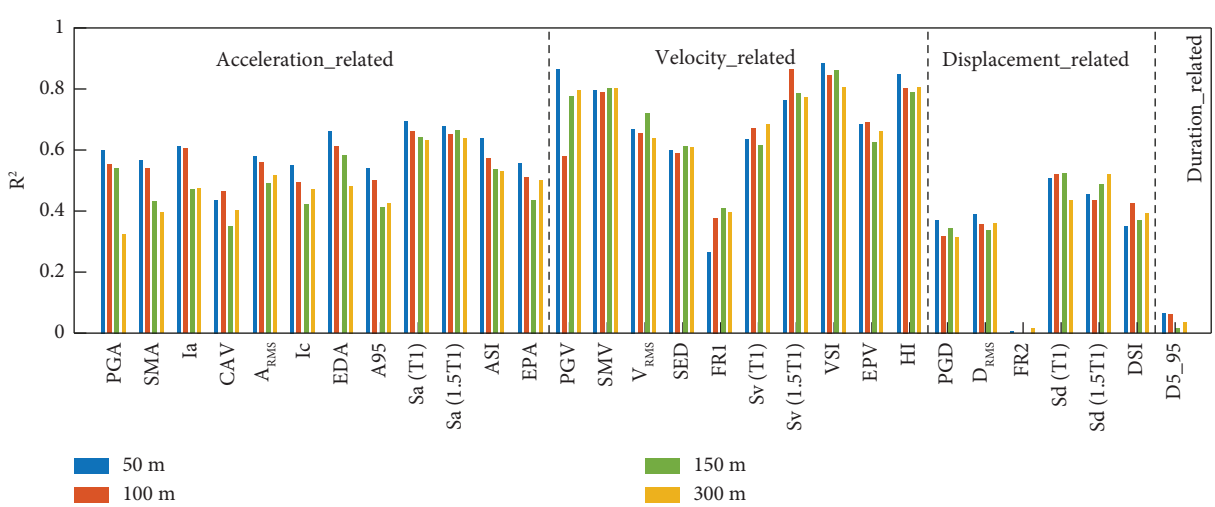

Figure 8: Correlation comparison of 29 candidate IMs against FOS for the slopes with different mining depths.

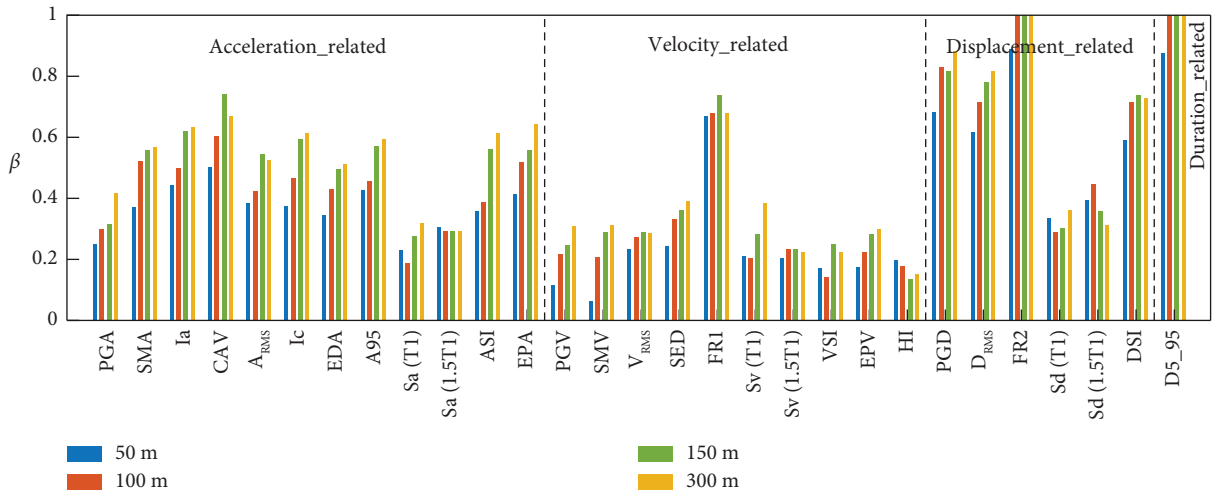

Figure 9: Efficiency comparison of 29 candidate IMs against FOS for the slopes with different mining depths.

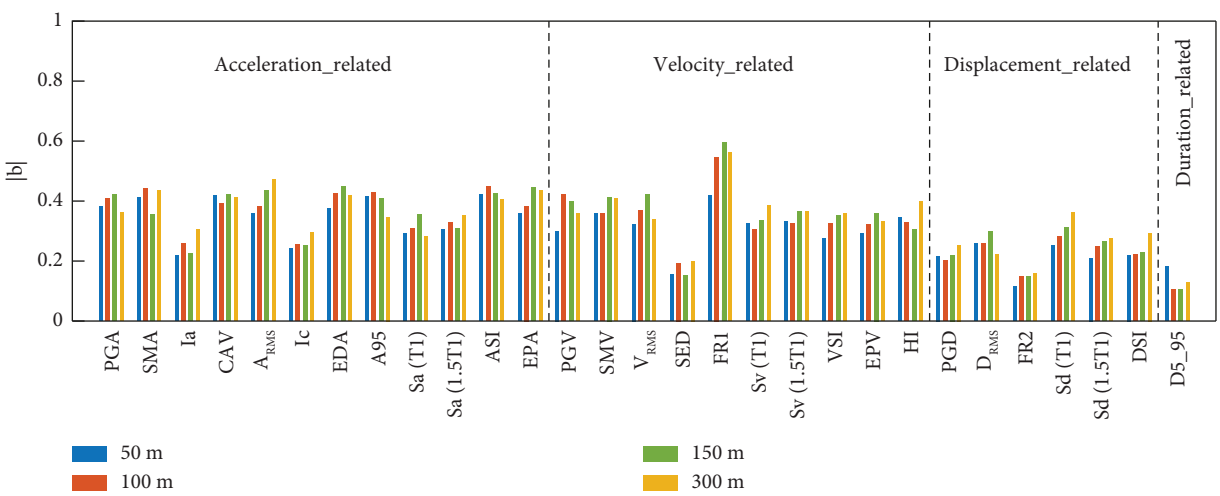

Figure 10: Practicality comparison of 29 candidate IMs against FOS for the slopes with different mining depths.

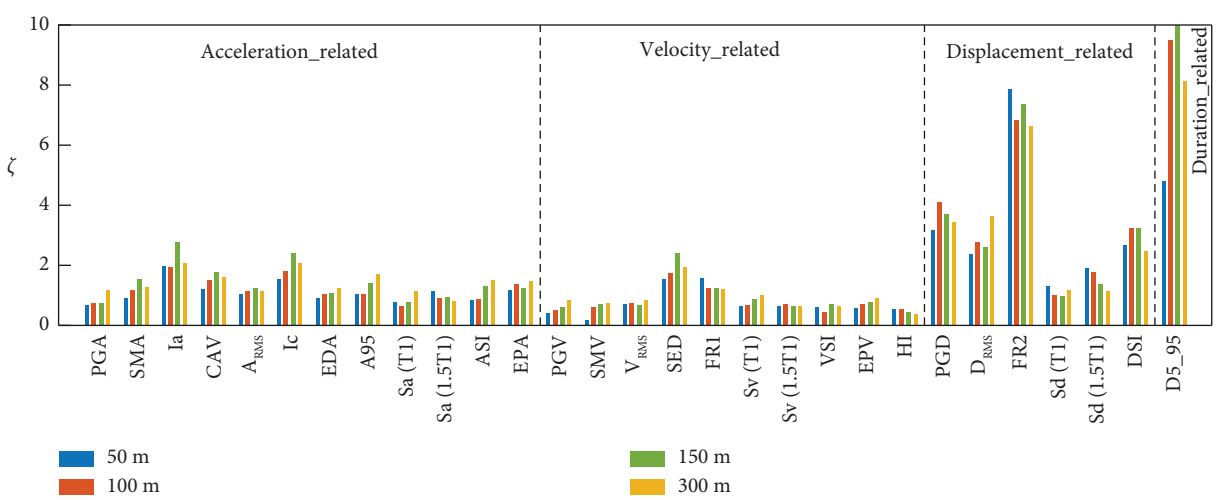

Figure 11: Proficiency comparison of 29 candidate IMs against FOS for the slopes with different mining depths.

three most proficient IMs for the slope with a mining depth of 300 m, and the ζ values are 0.377, 0.617, and 0.632. On the contrary, D_{5_95} and FR2 once again indicate the least proficiency with the corresponding ζ values of 8.126 and 6.631, respectively.

5.5. Sufficiency Comparison. To investigate the sufficiency of 29 candidate IMs, linear regression analysis between the residuals (denoted as $\varepsilon_{EDP|IM}$) of PSDMs and seismological parameters (i.e., magnitude M and source-to-site distance R) is performed. Here, moment magnitude M_w and rupture distance R_{rup} are chosen as the indicators of magnitude and source-to-site distance, respectively. The p value obtained from the regression results with respect to M and R is used to quantify the sufficiency of an IM. The p value ranges from 0 and 1. A more sufficient IM, which has a higher p value, is independent of seismological parameters. A significant level of 0.05 is considered in this study as the threshold for a sufficient IM. That is, an IM with p value less than or equal to 0.05 are assumed to be insufficient. Figure 12 depicts the linear regression results of top 1 sufficient IM associated with the M and R for the slope with a mining depth of 50 m. The slope factors of the regression lines are close to zero; whereas the p values are considerably higher. Therefore, it can be concluded that a best sufficient IM with respect to a seismological parameter has a higher p value and lower slope factor of the regression line.

The sufficiency of 29 candidate IMs with respect to M and R using p value is summarized in Figures 13 and 14. A p value level of 0.05 is plotted with a pink dash line. For all the slope cases with different mining depths, PGV, Sv ($1.5T_1$), SMV, and VSI are the most sufficient IM with respect to M, and HI, ASI, and PGV indicate the best sufficiency with respect to R. On the contrary, CAV, Ia, and D_{5_95} are the most insufficient with respect to M and R. It is also noted that PGA is insufficient with respect to M for the cases of 50 m and 100 m and slightly sufficient with respect to R, except for the case of 300 m.

According to the above-given analyses, Figure 15 presents top 3 correlated, efficient, practical, proficient, and sufficiency IMs for the open-pit slopes with different mining depths. It can be observed that optimal seismic IM varies with different criteria and mining depths. The optimal IMs based on correlation are consistent with the ones of efficiency. Therefore, proficiency, which combines of efficiency and practicality, is taken as the most critical criterion in this study, and sufficiency is considered as a supplementary requirement. By weighing various factors comprehensively, HI, VSI, and SMV can be selected as the appropriate IMs for the development of PSDM and fragility function of open-pit slopes with different mining depths in engineering practice. Among the three commonly used IM, PGV is superior to PGA and Sa (T_1).

5.6. Impact on Fragility Evaluation. In the following section, the seismic fragility curves using different IMs are further compared. Seismic fragility of a slope for a certain damage state is defined as the conditional probability of exceeding the specified damage level for a given seismic IM level. Fragility curves can be expressed by cumulative distribution function as follows:

$$F_{DS|IM} = P[DS \geq ds|IM] = \Phi\left(\frac{\text{In}(IM) - \text{In}(\mu_{IM})}{\beta_{IM}}\right), \tag{11}$$

where FDS|IM is the conditional probability at a given IM for a specified damage state ds. μ_{IM} is the median IM of a slope for a given damage state, and β_{IM} is the logarithmic standard deviation of IM conditioned on the given damage state.

Figure 16 shows the unacceptable fragility curves using top 1 IM and three commonly used IMs, i.e., PGV, PGA, and Sa (T_1), for the open-pit slopes with different mining depths. The values of unacceptable IMs are normalized to their corresponding median unacceptable IM value. Hence, the logarithmic standard deviations β_{IM} of the fragility curves using different IMs can be adopted as a quantitative comparison of the impact of IMs on fragility curves. It can be observed that for the open-pit slopes, the fragility curve using top 1 IM is steeper than the ones using three common IMs, and the β_{IM} value obtained is smaller than the other ones. This suggests optimal IM is more accurate and allows for less uncertainty in seismic fragility evaluation. It can also be found that the same results obtained for almost all other candidate IMs. In the three common IMs, PGV provides smaller β_{IM} values and less uncertainty than PGA and Sa (T_1).

5.7. Impact on FOS Hazard Evaluation. In PBEE framework, seismic response hazard integrates the seismic hazard analysis and seismic demand analysis. It provides the mean annual frequency (MAF) of exceeding certain seismic demand value given the seismic hazard at the designated site of a slope [61]. It can be calculated using the following equation:

$$\begin{aligned}\lambda(EDP > edp) = \int_0^{\infty} P[EDP > edp|IM \\ = im]|d\lambda(IM > im)|,\end{aligned} \tag{12}$$

where $|d\lambda(IM > im)|$ is the absolute value of the derivative of seismic hazard curve. $P[EDP > edp|IM = im]$ is the conditional probability of EDP exceeding edp given $IM = im$ and its full distributions constitute the fragility curves of more detailed damage states. If the EDP of interest is FOS, λ (FOS > fos) can be termed "FOS hazard." Assuming that seismic hazard function can be approximately expressed as the power form of equation (13) and the seismic demand values are log-normally distributed,

$$\lambda(IM > im) = k_0 \cdot IM^k, \tag{13}$$

where k_0 and k are two parameters representing the shape of the hazard curve.

Using the results of slope fragility curves as well as the seismic hazard curves of the site of interest, the FOS hazard curves can be calculated using equation (12). Based on the

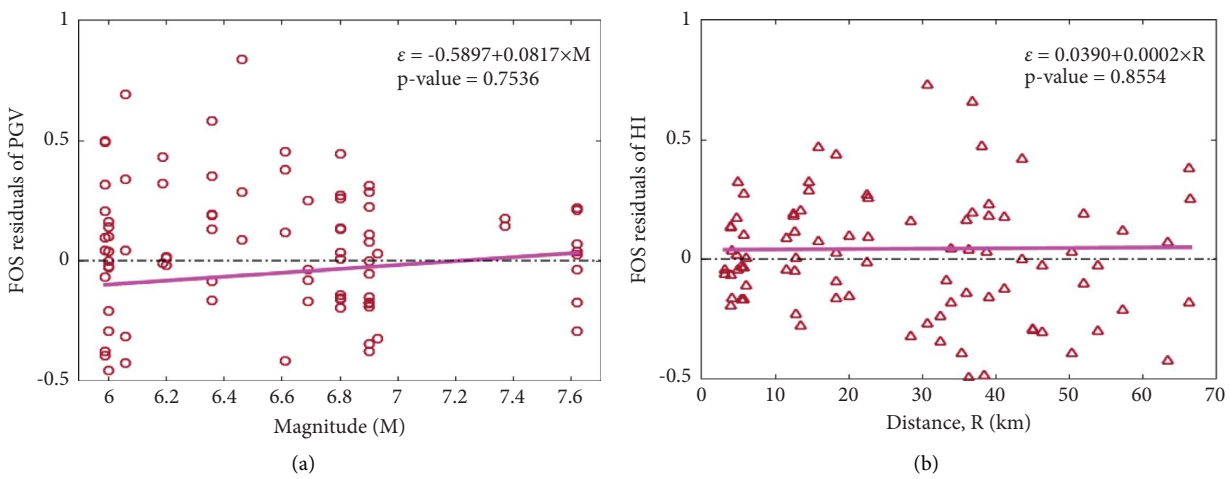

Figure 12: Illustration of IM sufficiency against M and R using p value for the slope with 50 m mining depth. (a) PGV with respect to M. (b) HI with respect to R.

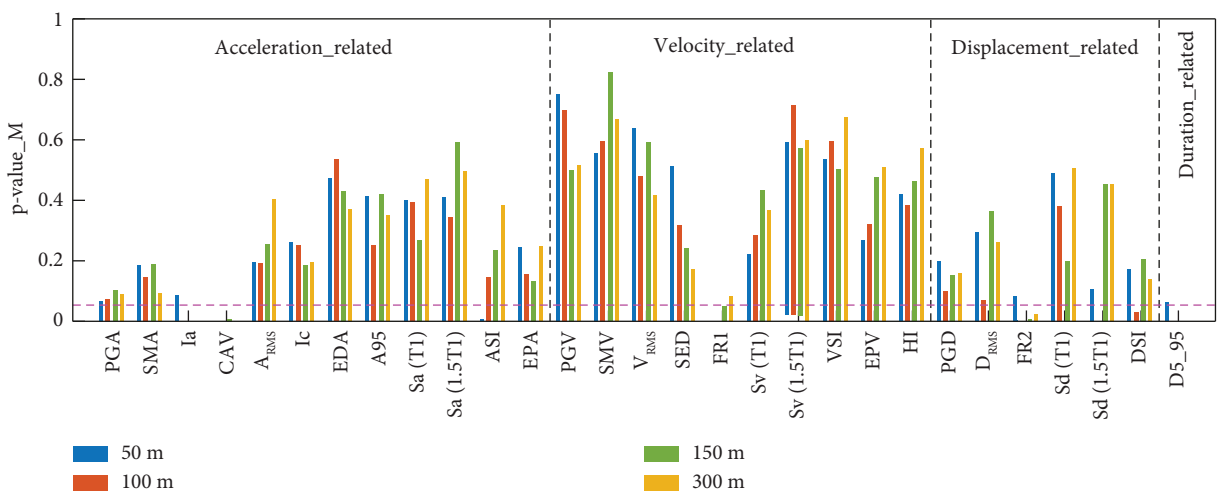

Figure 13: Sufficiency comparison of 29 candidate IMs against M for the slopes with different mining depths.

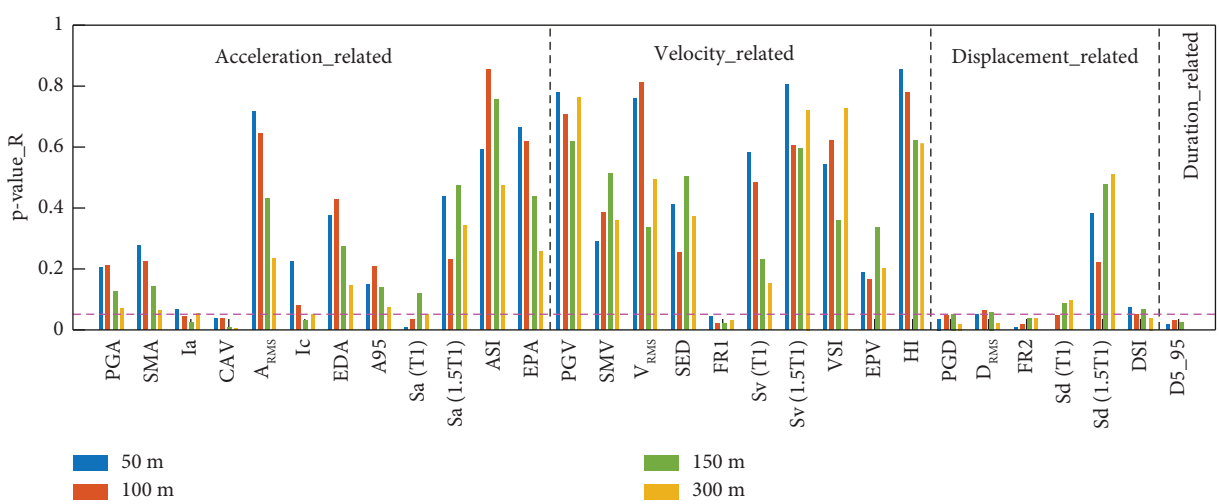

Figure 14: Sufficiency comparison of 29 candidate IMs against R for the slopes with different mining depths.

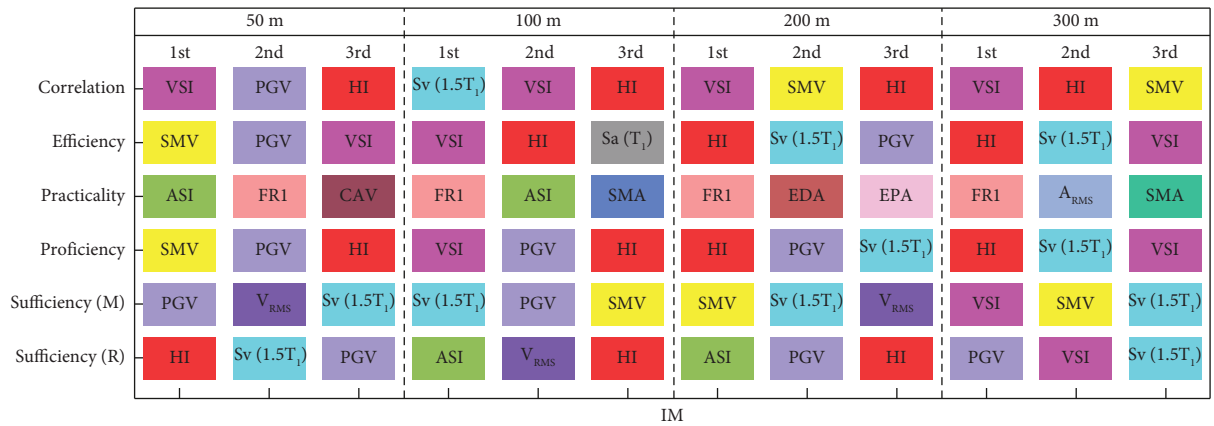

Figure 15: Top 3 correlated, efficient, practicable, proficient, and sufficient IMs for the slopes with different mining depths.

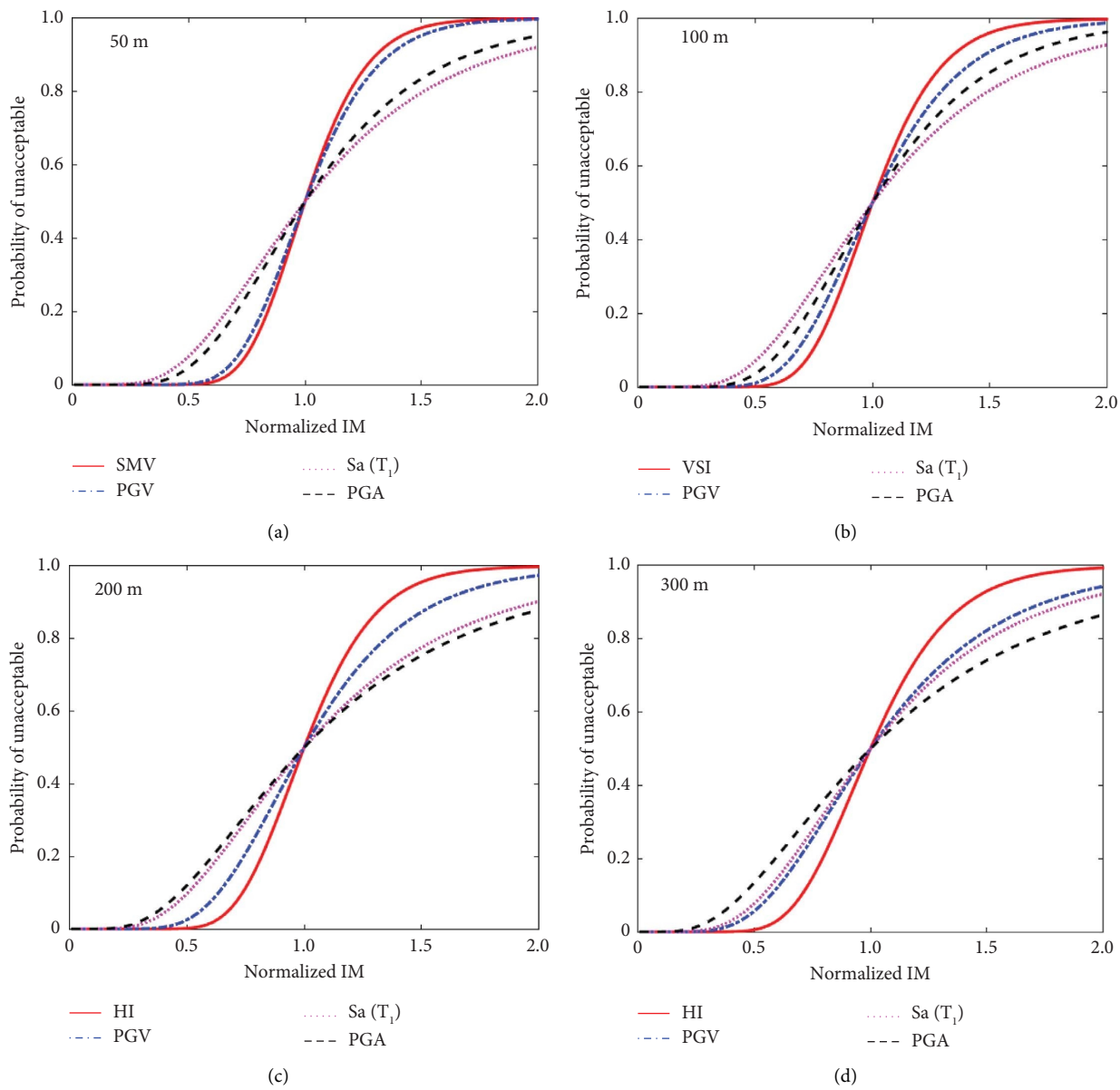

Figure 16: Unacceptable fragility curves using different IMs for the slopes with different mining depths. (a) 50 m. (b) 100 m. (c) 200 m. (d) 300 m.

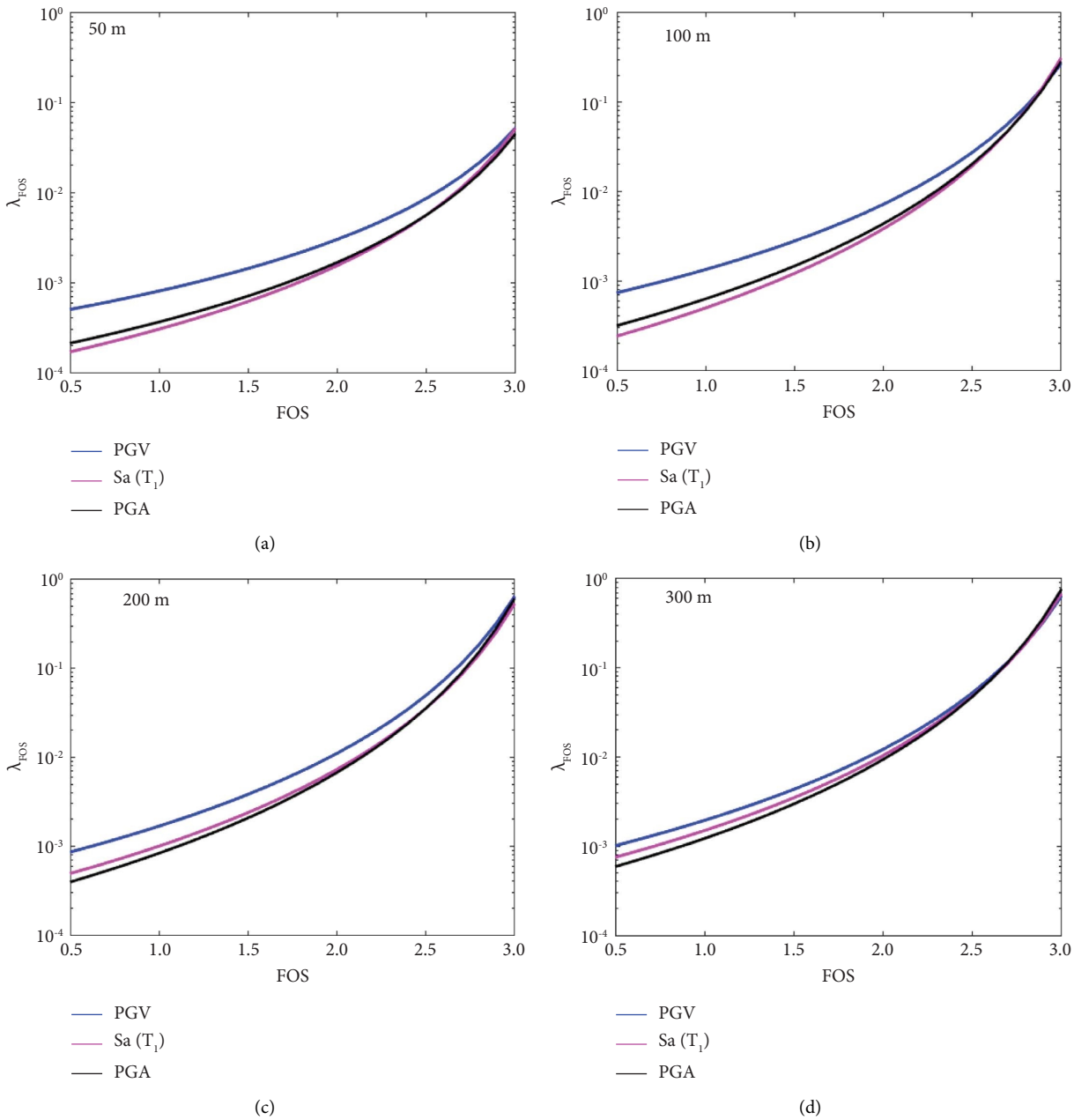

Figure 17: FOS response hazard curves using different IMs for the open-pit slopes with different mining depths. (a) 50 m. (b) 100 m. (c) 200 m. (d) 300 m.

above results, PGV is a relatively better IM among three commonly used IMs, especially for the slope cases with depths of 50 m and 100 m. Due to the lack of ground-motion prediction equations (GMPEs) for SMV, VSI, and HI in the region of interest [62, 63]. FOS hazard curves using PGV, PGA, and Sa (T_1) are obtained after all required parameters were determined, as shown in Figure 17. It indicates that the FOS hazard (i.e., the mean exceedance rate of FOS) using PGV is higher than the ones of PGA and Sa (T_1). For instance, the hazard response with FOS = 1.0 using PGV is 1.75 and 1.98 times the ones using Sa (T_1) and PGA for the slope with a mining depth of 50 m, respectively. However, the optimality of PGV decreases with the increase of mining depth, resulting in a gradual decrease in the gap of the FOS hazard curves using three common IMs. They illustrate that seismic IM has great influence on the FOS response hazard of the open-pit slopes. The gap may be even more pronounced when a better IM is used. Therefore, selecting the appropriate IMs, which is the main focus of this study, is essential to accurately evaluate the probabilistic seismic performance and dynamic stability of the open-pit slopes.

6. Conclusions

This study was mainly focused on the identification of optimal intensity measures (IMs) for probabilistic seismic stability and risk assessment of large open-pit mine slope within the framework of performance-based earthquake engineering (PBEE) methodology. Four two-dimensional numerical models of the open-pit slope cases with different mining depths were established by using the FEM software ABAQUS. The randomness of input bedrock ground motions and the uncertainty of rock properties of the slopes were also considered. Nonlinear time-history analyses of the open-pit slopes were performed under a total of 96 nonpulse earthquake records to capture the dynamic responses in terms of the minimum factor of safety (FOS). 29 candidate IMs against FOS were evaluated by five criteria including correlation, efficiency, practicality, proficiency, and sufficiency based on linear regression results of natural logarithmic space. Furthermore, the five damage states were defined based on the ranges of FOS of slopes. Seismic fragility curves and FOS hazard curves of the slope cases using different IMs were compared and discussed. Based on the investigated results, the mining depth of slopes has significant impacts on the identification of optimal IMs. More specifically, the following conclusions can be extracted:

Velocity-related IMs are better than the other three types of IMs for the open-pit slopes with different mining depths, and duration-related IMs and displacement-related IMs are the worst IMs. Furthermore, the optimality of most acceleration-related IMs decreases gradually with the increase of slope mining depth.

HI, VSI, and SMV can be taken as the best IMs for the development of PSDM and fragility function of open-pit slopes with different mining depth. On the contrary, FR2 and D_{5_95} are the most inappropriate IMs. PGV is superior to PGA and Sa (T_1) among the three commonly used IM.

The seismic fragility curves using optimal IMs are steeper than those of other IMs under a specified damage state, and the FOS response hazards using the more appropriate IM are higher than the other ones because the selection of an appropriate IM can greatly reduce the uncertainty of seismic fragility and seismic hazard of the open-pit slopes.

Note that, the investigated results presented in this study are for the factor of safety (FOS) of open-pit mine slopes using nonpulse ground motions. Future studies are necessary to reveal the impact of different EDPs (e.g., slope displacement) on the identification of optimal IM and the effect of near-fieldpulse-type ground motions.

Data Availability

The data used to support the findings of this study are available from the corresponding author upon request.

Disclosure

Any opinions, findings, and conclusions or recommendations expressed in this manuscript are those of the authors and do not necessarily reflect the views of the sponsors.

Conflicts of Interest

The authors declare that they have no conflicts of interest.

Acknowledgments

The authors thank Bin Zhang and Yajun Li for insightful reviews on an earlier version of this article. This study was financially supported by National Natural Science Foundation of China (Grant nos. 42107201 and 41572301) and Fundamental Research Funds for the Central Universities of China (Grant no. 2-65-2019-225).

References

[1] T. Carlà, P. Farina, E. Intrieri, H. Ketizmen, and N. Casagli, "Integration of ground-based radar and satellite InSAR data for the analysis of an unexpected slope failure in an open-pit mine," *Engineering Geology*, vol. 235, pp. 39–52, 2018.

[2] E. L. Harp and R. W. Jibson, "Landslides triggered by the 1994 Northridge, California, earthquake," *Bulletin of the Seismological Society of America*, vol. 86, pp. 319–332, 1996.

[3] K. Sassa, H. Fukuoka, G. Scarascia-Mugnozza, and S. Evans, "Earthquake-induced-landslides: distribution, motion and mechanisms," *Soils and Foundations*, vol. 36, pp. 53–64, 1996.

[4] M. Chigira, "Mountain hazards induced by the 1999 Chi-Chi earthquake and their change after the earthquake," *Journal of Japan Society for Natural Disaster Science*, vol. 28, no. 2, pp. 161–166, 2009.

[5] S. Qi, Q. Xu, H. Lan, B. Zhang, and J. Liu, "Spatial distribution analysis of landslides triggered by 2008.5.12 Wenchuan Earthquake, China," *Engineering Geology*, vol. 116, no. 1-2, pp. 95–108, 2010.

[6] L. Bo, Z. Peng, and Z. Jianwei, "Analysis on slope stability of open pit coal mine based on grey support vector machine," *International Journal of Smart Home*, vol. 10, no. 9, pp. 169–178, 2016.

[7] A. M. B. Al-Gharrawi and H. A. Abdulhusain, "Monte Carlo simulation for stability of finite slope subjected to earthquake loading," *IOP Conference Series: Materials Science and Engineering*, vol. 888, no. 1, Article ID 012010, 2020.

[8] T. T. Zhang, X. F. Guo, D. Dias, and Z. B. Sun, "Dynamic probabilistic analysis of non-homogeneous slopes based on a simplified deterministic model," *Soil Dynamics and Earthquake Engineering*, vol. 142, Article ID 106563, 2021.

[9] A. Filiatrault, D. Perrone, R. J. Merino, and G. M. Calvi, "Performance-based seismic design of non-structural building elements," *Journal of Earthquake Engineering*, vol. 25, no. 2, pp. 237–269, 2018.

[10] W. K. Lee and S. L. Billington, "Performance-based earthquake engineering assessment of a self-centering, post-tensioned concrete bridge system," *Earthquake Engineering & Structural Dynamics*, vol. 40, no. 8, pp. 887–902, 2011.

[11] D. S. Gao and J. R. Ye, "Earthquake resistance performance and reinforcement of soil-shell dam of Hualiangting Reservoir," *Chinese Journal of Geotechnical Engineering*, vol. 30, no. 12, pp. 1921–1924, 2008.

[12] B. Li, Q. H. Lai, E. D. Guo, C. X. Mao, and X. F. Li, "Determining the optimal scalar intensity measure of floor communication towers," *Shock and Vibration*, vol. 2022, Article ID 6347334, 12 pages, 2022.

[13] J. Macedo, J. Bray, N. Abrahamson, and T. Travasarou, "Performance-based probabilistic seismic slope displacement

procedure," *Earthquake Spectra*, vol. 34, no. 2, pp. 673–695, 2018.

[14] W. Yu and X. S. She, "Risk probability assessment of highway slope seismic disaster based on IDA-MC method," *Chinese Journal of Geological Hazard and Control*, vol. 28, no. 3, pp. 24–30, 2017.

[15] H. Q. Hu, Y. Huang, and Z. Y. Chen, "Seismic fragility functions for slope stability analysis with multiple vulnerability states," *Environmental Earth Sciences*, vol. 78, no. 24, pp. 690–710, 2019.

[16] X. Z. Wu, "Development of fragility functions for slope instability analysis," *Landslides*, vol. 12, no. 1, pp. 165–175, 2015.

[17] Z. K. Huang, D. M. Zhang, K. Pitilakis et al., "Resilience assessment of tunnels: framework and application for tunnels in alluvial deposits exposed to seismic hazard," *Soil Dynamics and Earthquake Engineering*, vol. 162, Article ID 107456, 2022.

[18] Z. K. Huang, S. Argyroudis, D. M. Zhang, K. Pitilakis, H. Huang, and D. Zhang, "Time-dependent fragility functions for circular tunnels in soft soils," *ASCE-ASME Journal of Risk and Uncertainty in Engineering Systems, Part A: Civil Engineering*, vol. 8, no. 3, Article ID 04022030, 2022.

[19] P. Giovenale, C. A. Cornell, and L. Esteva, "Comparing the adequacy of alternative ground motion intensity measures for the estimation of structural responses," *Earthquake Engineering & Structural Dynamics*, vol. 33, no. 8, pp. 951–979, 2004.

[20] E. I. Katsanos, A. G. Sextos, and G. D. Manolis, "Selection of earthquake ground motion records: a state-of-the-art review from a structural engineering perspective," *Soil Dynamics and Earthquake Engineering*, vol. 30, no. 4, pp. 157–169, 2010.

[21] N. D. Lagaros, Y. Tsompanakis, P. N. Psarropoulos, and E. C. Georgopoulos, "Computationally efficient seismic fragility analysis of geostructures," *Computers & Structures*, vol. 87, no. 19-20, pp. 1195–1203, 2009.

[22] M. Heshmati and V. Jahangiri, "Appropriate intensity measures for probabilistic seismic demand estimation of steel diagrid systems," *Engineering Structures*, vol. 249, Article ID 113260, 2021.

[23] M. Y. Xu, D. G. Lu, X. H. Yu, and M. M. Jia, "Selection of optimal seismic intensity measures using fuzzy-probabilistic seismic demand analysis and fuzzy multi-criteria decision approach," *Soil Dynamics And Earthquake Engineering*, vol. 164, Article ID 107615, 2023.

[24] F. Khosravikia and P. Clayton, "Updated evaluation metrics for optimal intensity measure selection in probabilistic seismic demand models," *Engineering Structures*, vol. 202, Article ID 109899, 2020.

[25] A. R. Tidke and S. Adhikary, "Optimal intensity measure selection and probabilistic seismic demand models for dam-reservoir-layered foundation system," *Structures*, vol. 37, pp. 318–337, 2022.

[26] K. Bakalis, M. Kohrangi, and D. Vamvatsikos, "Seismic intensity measures for above-ground liquid storage tanks," *Earthquake Engineering & Structural Dynamics*, vol. 47, no. 9, pp. 1844–1863, 2018.

[27] Z. K. Huang, K. Pitilakis, S. Argyroudis, G. Tsinidis, and D. M. Zhang, "Selection of optimal intensity measures for fragility assessment of circular tunnels in soft soil deposits," *Soil Dynamics and Earthquake Engineering*, vol. 145, no. 9, Article ID 106724, 2021.

[28] C. M. Zhang, M. Zhao, Z. L. Zhong, and X. L. Du, "Optimum intensity measures for probabilistic seismic demand model of subway stations with different burial depths," *Soil Dynamics and Earthquake Engineering*, vol. 154, Article ID 107138, 2022.

[29] S. Sarker, D. Kim, M. S. Azad, C. Sinsabvarodom, and S. Guk, "Influence of optimal intensity measures selection in engineering demand parameter of fixed jacket offshore platform," *Applied Sciences*, vol. 11, no. 22, Article ID 10745, 2021.

[30] S. Babaei, R. Amirabadi, T. Taghikhany, and M. Sharifi, "Optimal ground motion intensity measure selection for probabilistic seismic demand modeling of fixed pile-founded offshore platforms," *Ocean Engineering*, vol. 242, Article ID 110116, 2021.

[31] D. D. Nguyen, B. Thusa, M. S. Azad, V. L. Tran, and T. H. Lee, "Optimal earthquake intensity measures for probabilistic seismic demand models of ARP1400 reactor containment building," *Nuclear Engineering and Technology*, vol. 53, no. 12, pp. 4179–4188, 2021.

[32] D. D. Nguyen, T. H. Lee, and V. T. Phan, "Optimal earthquake intensity measures for probabilistic seismic demand models of base-isolated nuclear power plant structures," *Energies*, vol. 14, no. 16, p. 5163, 2021.

[33] J. D. Bray and T. Travasarou, "Simplified procedure for estimating earthquake-induced deviatoric slope displacements," *Journal of Geotechnical and Geoenvironmental Engineering*, vol. 133, no. 4, pp. 381–392, 2007.

[34] G. Wang, "Efficiency of scalar and vector intensity measures for seismic slope displacements," *Frontiers of Structural and Civil Engineering*, vol. 6, no. 1, pp. 44–52, 2012.

[35] T. Liang and J. Knappett, "Newmark sliding block model for predicting the seismic performance of vegetated slopes," *Soil Dynamics and Earthquake Engineering*, vol. 101, pp. 27–40, 2017.

[36] C. A. Cornell, F. Jalayer, R. O. Hamburger, and D. A. Foutch, "Probabilistic basis for 2000 SAC federal emergency management agency steel moment frame guidelines," *Journal of Structural Engineering*, vol. 128, no. 4, pp. 526–533, 2002.

[37] X. W. Wang, A. Shafieezadeh, and A. Ye, "Optimal intensity measures for probabilistic seismic demand modeling of extended pile-shaft-supported bridges in liquefied and laterally spreading ground," *Bulletin of Earthquake Engineering*, vol. 16, no. 1, pp. 229–257, 2018.

[38] W. Q. Du and G. Wang, "A one-step Newmark displacement model for probabilistic seismic slope displacement hazard analysis," *Engineering Geology*, vol. 205, pp. 12–23, 2016.

[39] C. C. Mitropoulou and M. Papadrakakis, "Developing fragility curves based on neural network IDA predictions," *Engineering Structures*, vol. 33, no. 12, pp. 3409–3421, 2011.

[40] Z. Y. Wang, N. Pedroni, I. Zentner, and E. Zio, "Seismic fragility analysis with artificial neural networks: application to nuclear power plant equipment," *Engineering Structures*, vol. 162, pp. 213–225, 2018.

[41] B. A. Bradley, M. Cubrinovski, R. P. Dhakal, and G. A. MacRae, "Intensity measures for the seismic response of pile foundations," *Soil Dynamics and Earthquake Engineering*, vol. 29, no. 6, pp. 1046–1058, 2009.

[42] N. Shome and C. A. Cornell, "Probabilistic seismic demand analysis of nonlinear structures RMS program," Report No. RMS35, Stanford University, Stanford, CA, USA, 1999.

[43] K. Mackie and B. Stojadinović, "Probabilistic seismic demand model for California highway bridges," *Journal of Bridge Engineering*, vol. 6, no. 6, pp. 468–481, 2001.

[44] J. E. Padgett, B. G. Nielson, and R. Desroches, "Selection of optimal intensity measures in probabilistic seismic demand models of highway bridge portfolios," *Earthquake Engineering & Structural Dynamics*, vol. 37, no. 5, pp. 711–725, 2008.

[45] N. Luco and C. A. Cornell, "Structure-specific scalar intensity measures for near-source and ordinary earthquake ground motions," *Earthquake Spectra*, vol. 23, no. 2, pp. 357–392, 2007.

[46] P. Tothong and N. Luco, "Probabilistic seismic demand analysis using advanced ground motion intensity measures," *Earthquake Engineering & Structural Dynamics*, vol. 36, no. 13, pp. 1837–1860, 2007.

[47] R. L. Wasserstein and N. A. Lazar, "The ASA statement on *p*-values: context, process, and purpose," *The American Statistician*, vol. 70, no. 2, pp. 129–133, 2016.

[48] N. Altman and M. Krzywinski, "Points of significance: P values and the search for significance," *Nature Methods*, vol. 14, no. 1, pp. 3-4, 2017.

[49] A. H. G. Mitchell, W. Myint, K. Lynn, M. T. Htay, M. Oo, and T. Zaw, "Geology of the high sulfidation copper deposits, monywa mine, Myanmar," *Resource Geology*, vol. 61, no. 1, pp. 1–29, 2010.

[50] Y. D. Zhou, P. Zou, F. F. Wang, Z. Liu, W. Hu, and Z. Ma, "Study on high and steep slope stability and slope angle optimization of open-pit based on limit equilibrium and numerical simulation," *Geotechnical & Geological Engineering*, vol. 38, no. 6, pp. 5737–5753, 2020.

[51] P. P. Martin and H. B. Seed, "One-dimensional dynamic ground response analyses," *Journal of the Geotechnical Engineering Division*, vol. 108, no. 7, pp. 935–952, 1982.

[52] Q. C. Lv, Y. R. Liu, and Q. Yang, "Stability analysis of earthquake-induced rock slope based on back analysis of shear strength parameters of rock mass," *Engineering Geology*, vol. 228, no. 10, pp. 39–49, 2017.

[53] K. K. Phoon and F. H. Kulhawy, "Characterization of geotechnical variability," *Canadian Geotechnical Journal*, vol. 36, no. 4, pp. 612–624, 1999.

[54] D. P. Dan, T. H. Ling, and F. Huang Fu, "Back analysis of strength parameters for the slip surface of stepped slope considering parametric," *Journal of Railway Science and Engineering*, vol. 16, no. 5, pp. 1186–1193, 2019.

[55] European Union, "Eurocode 8: Design of Structures for Earthquake Resistance, Part 5:foundations, Retaining Structures and Geotechnical Aspects," European Union, Brussels, Belgium, CEN-ENV 2004, 2004.

[56] Ministry of Housing and Urban-Rural Development of People's Republic of China, "Technical Code for Building Slope Engineering," Ministry of Housing and Urban-Rural Development of People's Republic of China, Beijing, China, GB 50330-2013, 2013.

[57] B. Li, Z. Cai, W. C. Xie, and M. Pandey, "Probabilistic seismic hazard analysis considering site-specific soil effects," *Soil Dynamics and Earthquake Engineering*, vol. 105, pp. 103–113, 2018.

[58] T. D. Ancheta, R. B. Darragh, J. P. Stewart et al., "NGA-West2 database," *Earthquake Spectra*, vol. 30, no. 3, pp. 989–1005, 2014.

[59] T. Travasarou, J. D. Bray, and N. A. Abrahamson, "Empirical attenuation relationship for arias intensity," *Earthquake Engineering and Structural Dynamics*, vol. 32, no. 7, pp. 1133–1155, 2003.

[60] Y. J. Kang, Y. Jun, and E. X. Song, "Calculation method and parameter research for time-history of factor of safety of slopes subjected to seismic load," *Rock and Soil Mechanics*, vol. 32, no. 1, pp. 261–268, 2011.

[61] B. U. Gokkaya, J. W. Baker, and G. G. Deierlein, "Quantifying the impacts of modeling uncertainties on the seismic drift demands and collapse risk of buildings with implications on seismic design checks," *Earthquake Engineering & Structural Dynamics*, vol. 45, no. 10, pp. 1661–1683, 2016.

[62] M. Petersen, S. Harmsen, C. Mueller et al., "Documentation for the southeast asia seismic hazard maps," Administrative Report, US Geological Survey, Reston, Virginia, 2007.

[63] B. Zhang, Y. X. Yu, X. J. Li, and Y. S. Wang, "Ground motion prediction equation for the average horizontal component of PGA, PGV, and 5% damped acceleration response spectra at periods ranging from 0.033 to 8.0s in southwest," *China Soil Dynamics and Earthquake Engineering*, vol. 159, Article ID 107297, 2022.